

ENCYCLOPEDIA OF EMULSION TECHNOLOGY

VOLUME 3

Basic Theory
Measurement
Applications

Edited by PAUL BECHER

Paul Becher Associates Ltd.
Wilmington, Delaware

This is a fac-simile of the last draft of this book chapter #2. You are intitled to consult this pdf version if your institution owns the book or if your are following a course taught by the author of this chapter.

MARCEL DEKKER, INC. NEW YORK and BASEL
1988

2

Phase Transformation and Emulsion Inversion on the Basis of Catastrophe Theory

JEAN-LOUIS SALAGER / Laboratorio FIRP, Escuela de Ingeniería Química, Universidad de los Andes, Mérida, Venezuela

1. Phase Behavior of Surfactant /Oil /Water Systems and Related Physicochemical Fundamentals	80
A. Surfactant /Oil /Water Systems	80
B. Interaction Energies	80
C. Phase Behavior of Sur fact ant /Oil /Water Systems	82
D. Optimum Formulation	86
E. Surfactant Affinity Difference Approach	89
F. Quality of an Optimum Formulation	92
II. Emulsion Inversion	94
A. Problems of Reproducibility	94
B. Emulsion Type and SOW Diagram	94
C. Bidimensional Formulation-WOR Diagram	98
D. Apparent Equilibration Time and Dynamic Inversion	102
III. Thermodynamic Modeling of Discontinuous Phenomena	105
A. Thermodynamic Approach to Emulsion Inversion	105
B. Catastrophe Theory Basics	105
C. Conventions	109
D. Application of the Cusp Catastrophe to Emulsions	111
E. Insufficiency of the Cusp Model	114
IV. Surfactant /Oil /Water Ternary Systems	114
A. Selection of a Catastrophe Theory Model	114
B. Interpretation of the Phase Behavior of SOW Ternaries	116
C. Interpretation of Emulsion Inversion	121
References	128

1. Phase Behavior of Surfactant /Oil /Water Systems, and Related Physicochemical Fundamentals

A. Surfactant /Oil /Water Systems

Surfactants are substances the molecules of which contain both polar and nonpolar groups. This dual character, called amphiphathy or amphiphilicity, results in a double affinity which can be satisfied only at a polar/nonpolar interface. The different types of surfactants and the general properties of surfactants in solution are covered in several books [1-11]; in this chapter it is assumed that the reader is familiar with such phenomena as adsorption, tensioactivity, and micellization [6,7,12-14].

In this chapter we deal with surfactant /oil /water (SOW) systems in a broad sense. The term water refers to a polar phase, which is in most applications an aqueous solution of electrolytes, while oil stands for a nonpolar phase essentially immiscible with water, such as a hydrocarbon, a triglyceride, other organic substances, or a complex mixture such as a crude oil. The surfactant may range from a pure isomeric species to a complex mixture of homologous or different amphiphilic substances. Often SOW systems contain an alcohol, which may act as a co-surfactant, and as a consequence may modify the behavior of the system. Alcohols tend also to have a physical effect, i.e. , they dissolve liquid crystal structures, and thus produce a simplification in the phase diagram [15,16]. As such they are used in many studies and applications. Alcohols do not alter the general phenomenology of phase behavior and emulsion properties presented here.

For the sake of simplicity, in this chapter we deal only with surfactant/oil/water (SOW) systems, keeping in mind that they correspond to pseudoternary systems in which each component may be a mixture. The pseudoternary approximation [17-19] results in a good representation when all the species of each pseudocomponent behave and fractionate in a collective way [20-22]. This is roughly true in a large majority of applications, where "water" is a brine, "oil" a mixture of nonpolar organic compounds, and "surfactant" a mixture of not-too-different species. When an alcohol is present its effect will be taken into account as an external effect, such as that of temperature.

B. Interaction Energies

Several decades ago, Winsor [6] introduced the concept of energies of interaction between the surfactant molecule adsorbed at the interface and both the oil and water phases. Figure 1 indicates the different types of interactions. C refers to the adsorbed surfactant layer, O to the oil phase, and W to the water phase. H and L represent the surfactant hydrophilic and lipophilic groups. Subscripts indicate the nature of interactions and/or the involved species. The ratio of the total interaction energies (per unit area of interface) of the surfactant for the O and W phases is known as Winsor R.

$$R = \frac{A_{CO}}{A_{CW}} \quad \text{or} \quad R = \frac{A_{LCO} + A_{HCO} - A_{OO} - A_{LL}}{A_{LCW} + A_{HCW} - A_{WW} - A_{HH}} \quad (1)$$

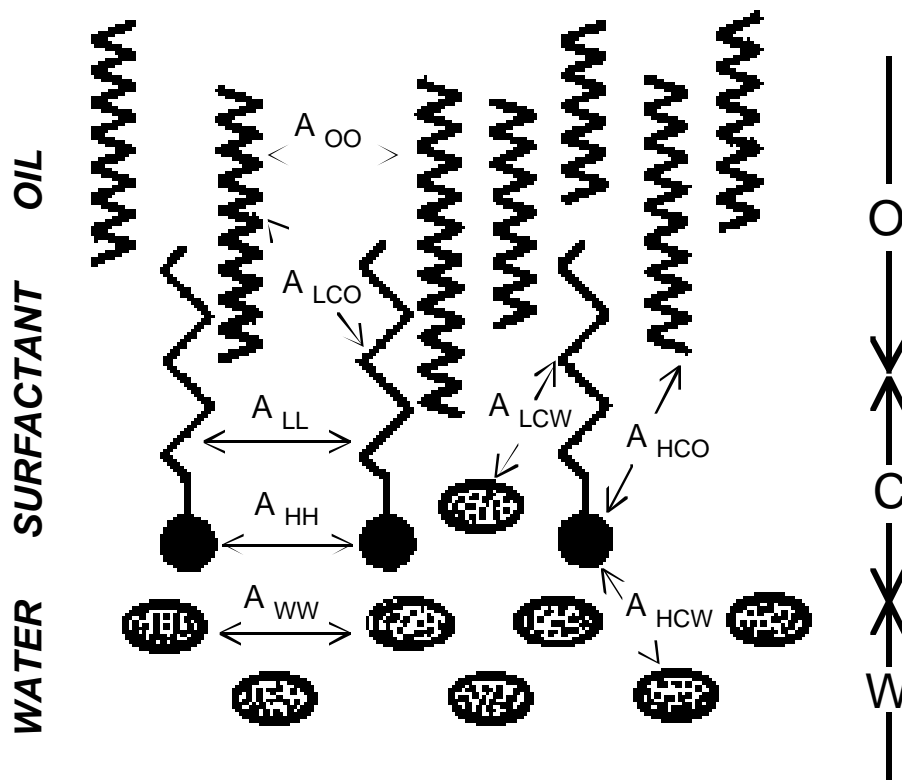


Figure 1. Different interaction energies according to the Winsor model.

The second expression is a refined definition which represents the overall net interaction balance between the surfactant and its physicochemical environment. It includes interactions that favor solvation (A_{LCO} , A_{HCW}) or oppose it (A_{OO} , A_{WW}). Both the value of the interactions and their overall ratio are of first importance for the topics dealt with in this chapter. Winsor's approach is purely qualitative, but has an exceptional pedagogical value because it clearly describes what is probably happening at the molecular scale. Recent researches [20,23-24] have shown that a refined Winsor R concept allows the interpretation of all known effects. Unfortunately, the energies of interaction are attainable neither by experiment nor by calculation, and as a consequence the Winsor R concept is of little help in practical applications.

With a completely different approach, Griffin introduced an empirical parameter, called the hydrophile-lipophile balance (HLB), in order to quantify the effect of the distinct interactions at interface [25,26]. The HLB is represented by an apparently arbitrary scale which actually equals one-fifth of the weight percent of oxyethylene in nonionic surfactants, such as polyoxyethylene alkyl phenols or fatty alcohols. The HLB of mixtures is estimated to a first approximation by a simple linear mixing rule based on weight fractions. Equivalent affinities toward the oil and water phases, i.e., unit Winsor ratio, roughly occurs around $HLB = 10$. It is worth noting that this balanced value corresponds to about 50% by weight of oxyethylene in polyoxyethylene alkyl phenols and fatty alcohols, a significant coincidence which may be used broadly as a rule of thumb. The HLB scale has been related closely to many experimental properties, and loosely to some fundamental concepts [27-42]. It is still widely used because of its simplicity, although it lacks accuracy and does not take into account the effect of variables such as salinity of the aqueous phase, alcohol content, or temperature [43-47].

With the intent of quantifying the Winsor R concept and linking it with Griffin's HLB, Beerbower and Hill introduced the cohesive energy ratio (CER) concept [35,48,49], which is based on the framework of the Hildebrand theory of regular solutions [50,51]. The CER is related to the solubility parameter, which may be calculated from experimental data [52]. However, so many questionable assumptions have to be applied in the SOW case that the usefulness of the CER is doubtful for such systems. It is thus desirable to explore other ways to quantify the balance of interaction energies at the interface. A thermodynamic approach is proposed below as an alternative, following the discussion of phase behavior.

C. Phase Behavior of Surfactant /Oil /Water Systems

Actual systems contain much more than three components. However, their phase behavior may be generally depicted, at least locally or by means of pseudo-components [18], by the idealized SOW ternary cases described by Winsor [6]. These diagrams will be dealt with in this chapter as typical, and it is worth noting that they must be the first ones to be explained by any new approach.

The behavior of these SOW systems may be viewed as a particular case of the general behavior of ternaries [17], where two of the components are essentially immiscible (O-W), whereas the two other pairs are fully miscible (S-W and S-O). As a consequence, the phase diagram exhibits a multiphase region only in the neighborhood of the O-W side. Near the S-W and S-O sides, and beyond a certain amount of S, the system behaves as a monophasic.

Winsor found that there were three different types of phase diagram, depending on the relative values of the interaction energies of the surfactant with the oil and water phases, i. e., its balance of affinity. Hundreds of experimental studies confirmed this classification, at least on a qualitative basis or in the local description of pseudoternaries [17, 19, 24, 53-62].

Figure 2 indicates the typical phase behavior in a Winsor Type I diagram, which corresponds to the case where the affinity of the surfactant S for the W (aqueous) component exceeds its affinity for the O (oil) component, i. e., for $R < 1$. Such a diagram exhibits a two-phase region near the O-W side, in which the tie lines slope indicates that most of the surfactant partitions into the aqueous phase. Such a two-phase region is referred to as $\underline{2}$, the mnemonic symbol [53] meaning two phases, most of the surfactant in the lower, i.e., more dense aqueous phase. Any system with an overall composition represented by the point c (square) in the two-phase region splits into two phases, whose compositions are located on the binodal boundary at the ends of the tie line passing through c: a surfactant-rich aqueous microemulsion (point a) and an excess oil phase (point o). Above the binodal boundary, one-phase systems are either micellar solutions near the O or W vertices, or microemulsions in the center of the diagram; depending on the nature of the components, especially the surfactant, mesophase structures such as liquid crystals or gels may also occur; however, they are beyond the scope of this chapter.

Winsor Type II diagram corresponds to the case in which the affinity of the surfactant for the oil phase exceeds its affinity for the aqueous phase, i.e., for $R > 1$. It is similar to Type I but with O and W roles inverted.

The two-phase region is referred to as $\bar{2}$, which mnemonic key [53] indicates two phases, most of the surfactant in the upper, i. e., less dense oil phase. A system with overall composition represented by the square (point c) inside the two-phase region splits into an oleic microemulsion (point o) which contains most of the surfactant, and an excess aqueous phase (point a).

It may be thought that the intermediate case between Type I and Type II, i. e., $R=1$, would exhibit a similar ternary diagram with horizontal tie lines, as a consequence of the exact balance of affinities of S for O and W. Such a situation does not occur for SOW ternaries in which the surfactant is either a pure component or behaves as a pseudocomponent. A Winsor Type III diagram (see Fig. 2) is obtained instead, in which the multiphase region is embodied by a three-phase zone surrounded by three two-phase zones [6]. Any system with an overall composition represented by c inside region 3 splits into three phases: a microemulsion (point m) which contains most of the surfactant and large amounts of solubilized oil and water, and two excess phases (points o and a). Such a decomposition indicates that the Gibbs free energy of the three-phase m-o-a system is lower than that of a hypothetical two-phase system with equal partitioning of the surfactant. The microemulsion phase is often referred to as *middle phase* [63], since its intermediate density makes it appear in a test tube between the aqueous and oil excess phases. It is also called the *surfactant phase* [64].

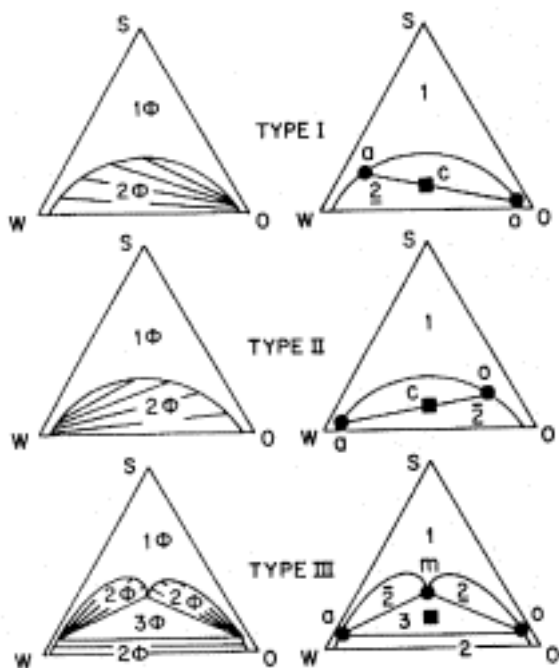


Figure 2. The three types of Winsor diagrams.

It has been found experimentally that the concentration of the surfactant in the o and a excess phases is roughly the same (for ionic surfactants) and that this value is about the critical micelle concentration in a similar aqueous environment, i.e., very low for most surfactants [21, 22, 54, 65, 66]. As a consequence, the lower two-phase zone (2) occupies a narrow strip between the almost horizontal a-o tie line and the W-O side. On an actual scaled diagram it essentially vanishes; however, it is worth noting that region 2 must exist for the sake of continuity down to the W-O side.

Above the om and am sides of the three-phase tie triangle, the Winsor Type III diagram exhibits two regions, with respective phase behavior of the $\underline{2}$ and $\bar{2}$ types similar to the ones observed in Type I and II diagrams. It should be pointed out that the phase splitting in these regions would result in an extremely swollen microemulsion phase. For example, the microemulsion phase obtained from phase splitting of a system with an overall composition in the left two-phase lobe $\bar{2}$ may contain more water than oil, in spite of being the "oil" phase of the two-phase system, the water phase being represented by a point near point a. In the Type III diagram represented in Fig. 2, the point representing the middle-phase micro-emulsion (m) is located on the median of the W-O side, i. e., this microemulsion contains equal amounts of water and oil. This is merely the symmetrical case; point m may be located almost anywhere between a and O.

Figure 3 shows the typical variation of the phase diagram of SOW systems when the nature of one of the components is changed in a monotonic way. In the illustrated case the oil phase is modified from hexane to tridecane (left to right) and the nature of the oil is indicated by its alkane carbon number ACN. When oil ACN increases, the affinity of the surfactant for the oil phase decreases as the oil becomes a poorer solvent, while its affinity for the aqueous phase remains unchanged since the aqueous phase is not altered. As a consequence, the overall balance of affinity of the surfactant varies from lipophilic (preference toward oil) at ACN 6, to hydrophilic (preference to water) at ACN 13. At low ACN Type II diagrams occur, whereas Type I diagrams are found at high ACN. In the midrange ($8 < \text{ACN} < 11$) Type III diagrams appear. The whole sequence indicates how the II-III-I transition takes place as ACN increases. The representative microemulsion (point m) moves from o to a (see Fig. 2), while the three-phase tie triangle increases and then decreases. For ACN value between 7 and 8 a $\underline{2}$ two-phase lobe starts forming, whereas the $\bar{2}$ two-phase region of the Type II diagram becomes a lobe above the

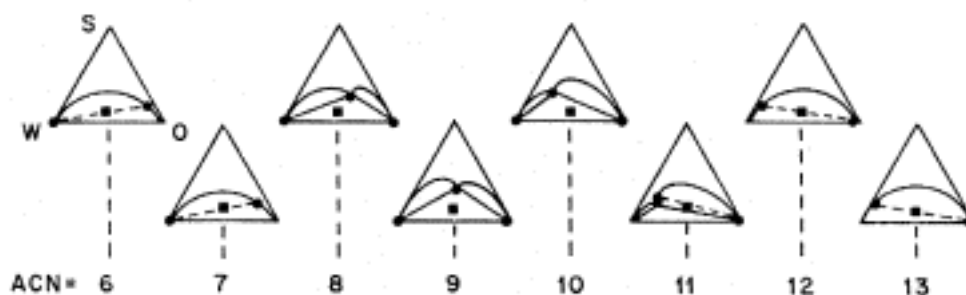


Figure 3. SOW ternary diagram transition when oil ACN increases. From left to right relative lipophilicity of the surfactant decreases.

three-phase region of the Type III diagram. As the ACN further increases, the $\bar{2}$ lobe shrinks while the $\underline{2}$ lobe expands as a consequence of the leftward shift of point m. For an ACN value between 11 and 12 the $\underline{2}$ lobe spreads over the whole multiphase region.

Such ternary diagram, transition, or its opposite, takes place whenever a variable capable of altering the affinity balance of the surfactant is scanned [21, 47, 55, 57, 67-69]. These so-called formulation variables were found to be:

- i. The salinity of the aqueous phase (type or concentration of electrolyte)
- ii. The nature of the oil (its ACN, or equivalent EACN when it is not an alkane)
- iii. The surfactant nature or HLB (in homologous series its molecular weight, in a mixture its composition, etc.)
- iv. The alcohol type or concentration
- v. The temperature, especially with nonionic surfactants

The first three variables match the nature of the ternary components, while the last two correspond to overall conditions and are thus labeled external variables [21,57, 69]. Of course, the alcohol type and concentration may be included as formulation and composition variables if a quaternary representation is used [56, 59, 70-73]; however, this is beyond the scope of this chapter.

The simplest way to determine the phase behavior of a system is by visual inspection of test tubes containing series of systems, the compositions of which are located at the nodes of a grid spread all over the diagram [55, 59]. Such a method requires a large number of experiments (100 to 200) to determine the phase boundaries of each diagram with some accuracy. A less time-consuming technique consists of diluting a one-phase system located slightly above the binodal curve with O and W aliquots in a constant ratio [56]. When the system becomes turbid, the multiphase region boundary has been crossed and the phase behavior type may be deduced from observation of the phase volumes. Depending on whether the new phase, i. e., the smaller volume phase, appears as a upper, lower, or middle phase, the phase behavior just below the multiphase boundary is $\underline{2}$, $\bar{2}$, or 3. The latter method typically needs at least three to five starting monophasic systems, three dilution O/W ratios for the aliquots, and the addition of about five aliquots for each of the previous settings. It is less time-consuming than the grid technique, but still requires several hours of experimental work for each diagram.

In many cases the information of interest is not the exact location of the multiphase region boundary, but rather, the type of diagram, i. e., the type of phase behavior inside the multiphase region. In such cases the determination of the phase behavior of a single system per diagram is sufficient, provided that the representative point of the overall composition of the selected system lies inside the multiphase zone, i. e., the square point in Figs. 2 and 3. Experience shows that such a system should contain 0.5 to 3% (recommended 1%) of surfactant [21, 53, 55]. At much lower surfactant concentration, the middle phase volume, which is roughly proportional to the surfactant content, might not be easily detectable; at high surfactant concentration, the representative point of the system may be located above the multiphase boundary.

On the other hand, it is recommended that systems with equal amounts of O and W be used, for reasons that will become clear later.

Under these conditions, the determination of the phase behavior of a single system per diagram, i. e., per formulation, allows the rapid estimation of the diagram type. In, the case of Fig. 3 it is clear that the phase behavior for a composition represented by the square fits the diagram type in all but the ACN 11 case, where a type 2 observed phase behavior actually corresponds to a Type III diagram. However, the large swelling of the microemulsion phase might give a hint to a seasoned experimenter about the actual situation. In any case, the selection of a unit water/oil ratio would ensure that such a slight error similarly happens at both I-III and II-III transitions, and as a consequence, they cancel each other out in the determination of the center of the range of values of the scanned variable, for which three phases are exhibited. This center value, called the *optimum formulation* of the scan, is the parameter of interest.

D. Optimum Formulation

In the past 10 years considerable research effort has been carried out at universities and industrial laboratories in order to understand the phenomena involved in the enhanced oil recovery process called surfactant or micellar flooding [74-77]. It was found that three-phase behavior is associated with ultralow interfacial tension, i.e., the physico-chemical condition to offset the capillary forces which maintain the residual oil trapped in the porous matrix of a reservoir [78-81]. The attainment of an ultralow interfacial tension matches the maximum oil recovery, and as a consequence the corresponding formulation is referred to as "optimum" [55, 74-76, 82].

An optimum formulation is found by scanning one of the formulation variables while all others, including the composition variables, are held constant. Figure 4 shows some of the phenomena observed in a formulation scan. The test tube illustration indicates the observed phase behavior; the shaded area represents the surfactant-rich microemulsion (m), while symbols o and a identify the excess oil and aqueous phases. In the three-phase range there are two interfaces: the upper one (om) between the microemulsion and the excess oil, and the lower one (ma) between the microemulsion and the excess aqueous phase. Above and below the test tube, the phase behavior and the corresponding type of Winsor diagram are indicated. The solubilization parameters indicate the volume of one of the components, either O or W, solubilized in the microemulsion phase per unit mass of surfactant.

In the three-phase range two interfacial tensions and two solubilization parameters coexist. The optimum formulation of the scan is located at or near the center of the three-phase range, which essentially corresponds to the crossing point of the tension and solubilization parameter curves. At the transition, a strong change takes place in the partition coefficient of the surfactant between the o and a phases [21, 661]. The partition coefficient between the excess phases is roughly unity (with ionic surfactants), in three-phase systems [22, 65, 661]. Such a phenomenology has been found by scanning all formulation variables, and additional properties of optimum formulation systems have been reported [55, 82-90].

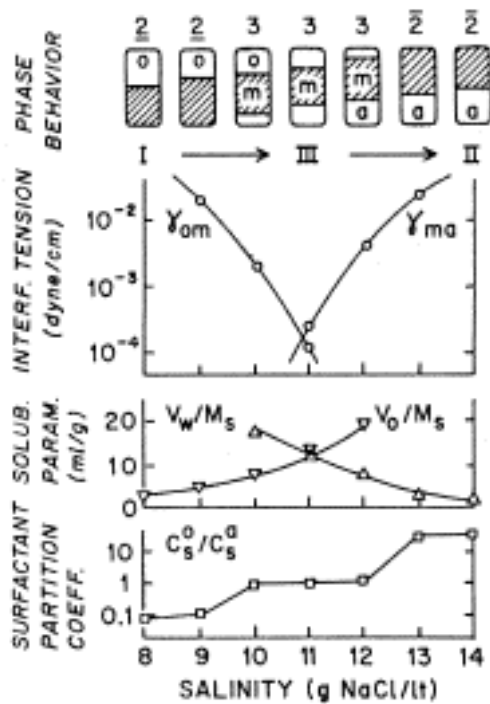


Figure 4. Formulation (salinity) scan showing the effects of the $\underline{2}$ - 3 - $\bar{2}$ transition on several properties. System Witco TRS-80/octane. (From Ref. 21.)

Extensive experimental studies [20, 24, 55, 59, 62, 84, 91-104] have shown that an optimum formulation is attained whenever a certain relationship is fulfilled by the formulation variables. For anionic surfactants Salager and co-workers [21, 57, 102] found that the following correlation was required for optimum formulation to occur:

$$+ \ln S - K \text{ EACN} - f(A) + a_T (T - 25) = 0 \quad (2)$$

where K is a characteristic parameter of the surfactant, $\ln S$ the natural logarithm of the salinity of the aqueous phase (S expressed in weight percent of sodium chloride), EACN or equivalent alkane carbon number a measurement of the lipophilicity of the oil phase [94, 104-107], $f(A)$ a graphed function of alcohol type and concentration, and T the temperature in $^{\circ}\text{C}$. The constant K depends on the type of hydrophilic group of the surfactant and a_T is a temperature shift coefficient.

For ethoxylated nonionic surfactants Bourrel and co-workers [69, 101, 108, 109] reported a similar correlation:

$$- \text{EON} - k \text{ EACN} + mA_i + bS + C_T (T - 28) = 0 \quad (3)$$

where k depends on the lipophilic group of the surfactant, EON is the average number of ethylene oxide groups per surfactant molecule, and A_i stands for the alcohol concentration.

Parameters m and b depend on the type of alcohol and electrolyte, respectively, and k and C_T are constants. The effects of water/oil ratio and surfactant concentration may be taken into account by corrective terms [21, 46, 47].

Both correlations for optimum formulation may be written as linear relationship between the formulation variables [58]:

$$L = \sum_{i=1}^{i=n} C_i X_i = 0 \quad (4)$$

where X_i stands for the formulation variables and C_i their associated coefficients. Depending on the sign of L , the observed phase behavior is $\underline{2}$ ($L < 0$), $\bar{2}$ ($L > 0$), or 3 ($L = 0$). This relationship may be written in the following way, by isolating a pair of formulation variables, X_1 and X_2 :

$$C_1 X_1 + C_2 X_2 = - \sum_{i=3}^{i=n} C_i X_i \quad (5)$$

By keeping the last $(n - 2)$ X_i constant, the right-hand term remains constant and an optimum formulation is attained whenever the linear relationship between X_1 and X_2 is verified. This is shown in Fig. 5 using $\ln S$ and ACN as variables for an anionic system where the center line of the three-phase region represents the linear relationship. It is thus clear that the change in one of the formulation variables may be compensated by a change of any other in order to maintain an optimum formulation. The effects of the formulation variables are thus independent and additive. This undoubtedly suggests the features of Winsor's interaction energies, and it is worth trying to analyze this analogy by means of a thermodynamic approach.

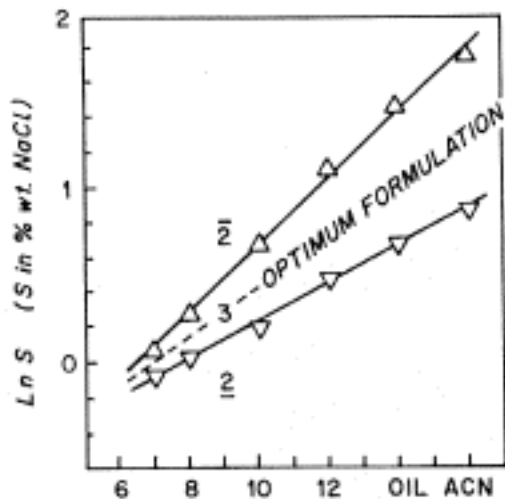


Figure 5. Phase behavior in $\ln S$ -ACN subspace. System Witco TRS 10-80/sec-butanol/alkanes. (From Ref. 21.)

E. Surfactant Affinity Difference Approach

Let μ be the chemical potential of the surfactant and μ^* its value in some reference state to be selected later.

$$\mu_w = \mu_w^* + RT \ln x_w a_w \quad (6)$$

$$\mu_o = \mu_o^* + RT \ln x_o a_o$$

where the subscripts refer to the phase, x represents the relative concentrations, and a the activity coefficients. Let x be C/C^* , where C^* is a surfactant reference concentration which is low enough so that the activity coefficients are unity at $C=C^*$, i. e., at $x = 1$. The symbol μ^* represents the standard chemical potential in this reference state; it depends on all formulation variables but is independent of the surfactant concentration.

At equilibrium the chemical potential of the surfactant has the same value in all phases: $\mu_o = \mu_w$; thus

$$\mu_o^* - \mu_w^* = RT \ln (x_w a_w / x_o a_o) \quad (7)$$

From experimental evidence it is known that in a three-phase system the surfactant concentrations in the excess O and W phases are extremely low and roughly equal to each other (in ionic systems) [66]. They may be assumed to be low enough so that activity coefficients are unity. Condition (7) for optimum formulation thus becomes

$$\mu_o^* = \mu_w^* \quad (8)$$

From the physicochemical point of view, this means that at optimum formulation the affinity of the surfactant (negative standard chemical potential) toward the aqueous phase exactly equilibrates its affinity toward the oil phase [58, 66, 98]. A phenomenological variable may be defined as the surfactant affinity difference (SAD) [110] by

$$\text{SAD} = -\mu_o^* - (-\mu_w^*) = \mu_w^* - \mu_o^* \quad (9)$$

Depending on whether SAD is negative, positive, or near zero, the phase behavior is $\underline{2}$, $\bar{2}$, or 3, respectively.

It was mentioned previously that the phase behavior is studied by scanning a single formulation variable at a time. For instance, an increase of salinity produces the $\underline{2} \rightarrow \bar{2} \rightarrow 3$ transition, i.e., it increases the SAD value from negative to positive. Figure 6 illustrates the qualitative variations of the standard chemical potentials of the surfactant in a salinity scan. When the salinity of the aqueous phase increases, the standard chemical potential μ_w^* increases, whereas μ_o^* is not affected and remains constant. The surfactant affinity difference changes sign as expected, and the optimum formulation of the scan (Sopt) is obtained at the crossing of the two potential curves, i. e., at $\text{SAD} = 0$.

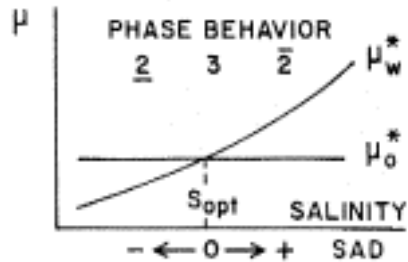


Figure 6. Variation of the standard chemical potentials through a salinity scan. (From Ref. 58.)

Figure 7 indicates the same variations, but this time for two salinity scans carried out at different values of ACN, all other variable being held constant. Since μ_o^* tends to increase with oil ACN, case (1) corresponds to the lowest ACN value and case (2) to the highest. The variation of μ_w^* does not depend on oil ACN and is thus represented by the same curve in both cases. The intersection point, i.e., the optimum formulation, is shifted from case (1) to case (2), so that a higher ACN effect is compensated by a higher salinity. This may be deduced readily from the application of correlation (2) to cases (1) and (2):

$$\ln S_1 - KACN_1 + Cst = 0 \quad (10)$$

$$\ln S_2 - KACN_2 + Cst = 0$$

It should be pointed out that the two optimum formulations are not identical, as will be discussed below when dealing with the concept of quality. In the (1)-(2) change, the optimum formulation is conserved, i.e., SAD remains equal to zero. For such an infinitesimal change

$$d\mu_o^* = d\mu_w^* \quad (11)$$

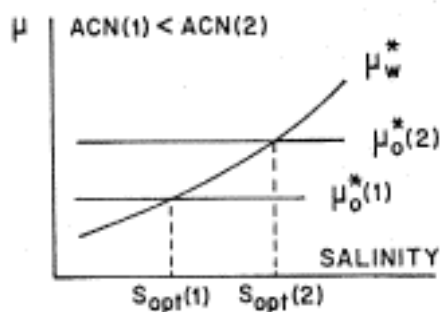


Figure 7. Variation of the standard chemical potentials through a salinity scan carried out at two different ACN values. (From Ref. 110.)

The variation of μ^*_o is due only to a change in ACN, while the variation of μ^*_w is produced by a change in $\ln S$.

$$d\mu^*_o = \frac{\mu^*_o}{ACN} dACN \quad \text{and} \quad d\mu^*_w = \frac{\mu^*_w}{\ln S} d\ln S \quad (12)$$

According to Eq. (10), the change should be such that

$$\ln S - KACN = Cst \quad \text{or} \quad d \ln S = K dACN \quad (13)$$

As a consequence, the partial derivatives are proportional to each other.

$$\frac{\mu^*_o}{ACN} = K \frac{\mu^*_w}{\ln S} \quad (14)$$

Since μ^*_o and μ^*_w are functions of different variables, the generality of Eq. (14) implies that the two partial derivatives are constant. By generalizing to other pairs of variables, each of the $d\mu^*$ can be written:

$$d\mu^* = \frac{\mu^*}{X_i} dX_i = b_i dX_i \quad (15)$$

where the X_i are the formulation variables involved in the correlation and the b_i are constant coefficients. By integration, a linear expression is obtained for both μ^* . By subtracting expressions for μ^*_o and μ^*_w a linear form is found for SAD.

$$SAD = \mu^*_w - \mu^*_o = b_i X_i \quad (16)$$

It may be shown by a straightforward algebraic manipulation [110] that this SAD expression is proportional term by term to the correlation for the optimum formulation, i. e., Eqs. (2)-(4). The proportionality constant may be reasonably selected as (RT) , so that, for example for anionic surfactant systems, SAD is expressed by

$$\frac{SAD}{RT} = \frac{\mu^*_w - \mu^*_o}{Rt} = \ln S - K EACN - f(A) + \quad + a_T (T - 25) = 0 \quad (17)$$

In other words, the empirical correlations (2) and (3) for the attainment of an optimum formulation represent a zero SAD (for ionic surfactant systems[†]), and each term corresponds to a specific contribution in the energetic balance. A posteriori, it is no wonder that the correlations are linear forms, i.e., combinations of independent and additive terms. As a consequence, an off-optimum formulation may be characterized by its SAD value, or its deviation from optimum formulation expressed as the algebraic value of the left-hand term of the correlation in Eqs. (2) and (3). SAD represents the same concept as the Winsor R ratio, but it is expressed in terms which are experimentally attainable and is therefore more useful for practical applications.

[†] This is not strictly true for nonionic surfactant systems in which the activity coefficient is very different from unity. In this case the definition of SAD is not in base of the ratio of concentrations, but the ratio of activities. Hence $SAD = RT \ln[Co/Cw] = SAD_{ref}$ is different from zero at optimum formulation. This does not change the concept, but allows for a more general dimensionless formulation concept, so-called Hydrophilic-Lipophilic Deviation $HLD = (SAD - SAD_{ref})/RT$

F. Quality of an Optimum Formulation

Because of the compensating effect of two or more formulation variables, several degrees of freedom are available in attaining an optimum formulation. Mathematically speaking, if n formulation variables are involved, the optimum formulation locus is represented by a hypersurface of dimension $(n - 1)$. As pointed out previously all these optimum formulations are not identical, as the experimental evidence indicates [23, 24, 111]. This may be ascertained easily in the example of Fig. 7, in which optimum formulation is maintained by compensating changes (1)-(2) of $\ln S$ and ACN.

In case (2) at the optimum formulation, both μ^*o and μ^*w are higher than in case (1); hence in case (2), the affinity of the surfactant for each phase is lower than in case (1). Thus case (2) corresponds to an optimum formulation of poorer "quality" than case (1). This concept of quality of an optimum formulation has not yet been fully defined but has been recognized in several studies. It may be easily linked with Winsor interaction energy ratio R . At optimum formulation the interactions are exactly balanced and thus $R = 1$; however, this unit value may be obtained as a balance between strong interaction energies, say the ratio 10/10, or between weak interactions energies, say the ratio 2/2.

A higher quality should correspond to higher interactions or higher affinity of the surfactant for both phases. As far as the physicochemical properties are concerned, a higher quality should match a lower interfacial tension minimum or a higher solubilization [23, 24, 55, 111-113]. Recent studies indicate that a high quality should also correlate with a low height of the multiphase region of the ternary diagram [114, 115] and a narrow three-phase range in a formulation scan [20, 116, 117]. The data of Fig. 5 indicate that the three-phase range increases linearly when $\ln S$ and ACN increase in a compensating way.

The very existence of the middle-phase microemulsion at optimum formulation actually seems to be linked to the concept of quality [109,118]. The occurrence of a microemulsion m in optimum three-phase systems implies that the surfactant exhibits a high affinity toward this structure [6, 89, 119,120]; that is, μ^*m is lower than both μ^*o and μ^*w . This is corroborated by the evidence that the surfactant seems trapped in the middle phase and is unavailable to stabilize a macroemulsion, as was recently reported [121-123].

The phase behavior variation through a salinity scan can be interpreted by adding to the previous SAD model an expression for the standard chemical potential of the surfactant in the microemulsion middle phase μ^*m . Near optimum formulation, i. e., near zero SAD, μ^*m must be lower than both other standard chemical potentials. Since the optimum formulation is generally at the center of the three-phase range, it is reasonable to choose a symmetrical parabolic expression such as [110]

$$\mu^*_m = K_1 + K_2 (\text{SAD})^2 \quad (18)$$

Figure 8 illustrates the variation of the three standard potentials along a formulation scan, for example an HLB scan. Depending on whether the lowest potential is μ^*w , μ^*m , or μ^*o , the phase behavior is $\underline{2}$, $\underline{3}$, or $\bar{2}$, respectively. The values of K_1 and K_2 in Eq. (18) may change the depth of the minimum and the width of the three-phase range.

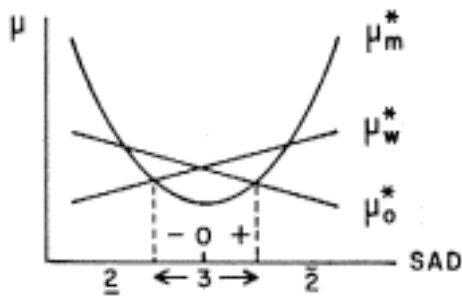


Figure 8. Variation of the standard chemical potential through a formulation scan, with a parabolic model for μ_m^* . (From Ref. 110.)

According to the fragmentary data available, a high-quality system should correlate to a deep and narrow μ_m^* parabola, i.e., low values of both K_1 and K_2 .

The experimentally found increase of width of the three-phase range with increasing salinity and ACN (see Fig. 5) is illustrated with this model in Fig. 9, which shows a formulation scan such as surfactant parameter a or HLB, referred to as SAD, for two different but compensating sets of values of ACN and $\ln S$, such that

$$\ln S_1 - KACN_1 = \ln S_2 - KACN_2 \quad (10)$$

In case (2) of Fig. 9, both salinity and ACN are higher than in case (1) as a consequence both μ_o^* and μ_w^* are shifted to higher values, but the position of their crossing point is not affected because of the compensating effects, i.e., $\ln S$ and ACN on SAD. For the sake of simplicity it is assumed (incorrectly) that the μ_m^* parabola shape is not affected by the $\ln S - ACN$ change. Actually, it should rise and widen from case (1) to (2). From Fig. 9 it is clear that the compensating change of $\ln S$ and ACN from (1) to (2) widens the three-phase range of SAD.

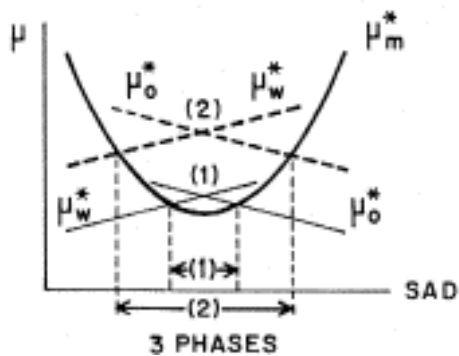


Figure 9. Variation of the three-phase range with a compensating change of salinity and ACN. (From Ref. 110.)

There is still a long way to go before a Gibbs free energy function, taking into account all formulation variables, can be constructed for a SOW system. However, the present approach indicates that at least in the neighborhood of an optimum formulation, the effect of the formulation may be rendered by a single generalized formulation variable, i.e., SAD. Also, it makes clear that $SAD = 0$ may be used as a reference state, and that the deviation from optimum formulation, i.e., the SAD value, may be used as a yardstick when comparing systems that possess completely different values of formulation variables. This represents quite a reduction in the number of variables involved, and thus a simplification in the description of the phenomenology, as the following will show.

II. Emulsion Inversion

A. Problems of Reproducibility

When scrutinizing the hundreds of articles on emulsions published in the past 50 years, the overall impression is that there are many discrepancies and too many exceptions to the general rules. Even the review texts [10, 11, 124] leave a feeling of haziness and unsettled comprehension when dealing with the effects of variables involved in the formulation. The preparation guidelines of commercial products often read like cooking recipes, to be followed strictly step by step in order to avoid drastic deviations from the desired result.

The principal problem seems to be the lack of consistency and reproducibility in the properties of supposedly similar or identical systems. A close examination of several cases of discrepancy indicated that most of the emulsions were prepared with SOW systems which were not previously equilibrated from the physicochemical point of view. Although the overall formulation may be well defined, the actual state of nonequilibrated system, especially the surfactant partitioning and adsorption, as well as related properties such as interfacial tension, may differ largely from case to case [125-127].

To avoid this source of difficulty and uncertainty, recent studies have dealt with emulsions prepared with SOW systems which are equilibrated prior to emulsification. Equilibration needs a typical 24-h contact between phases, although some systems may require much less or much more time. Such circumstances guarantee that systems with identical formulation and composition are in identical states at the moment the emulsification process is carried out. As will be seen in this section, this precaution allows rationalization of the formulation effects.

B. Emulsion Type and SOW Diagram

When emulsions are obtained from pre-equilibrated systems it is convenient to plot both the phase behavior and the emulsion type on a SOW ternary diagram. Macroemulsions are obtained when the representative point of the overall = composition of the system lies inside the multiphase region.

At each point of this region the equilibrated systems may be emulsified and the emulsion type determined. Assuming initially that an emulsion can be either only oil in water (O/W) or water in oil (W/O), the multiphase region may be divided in two areas according to the emulsion type (see Fig. 10).

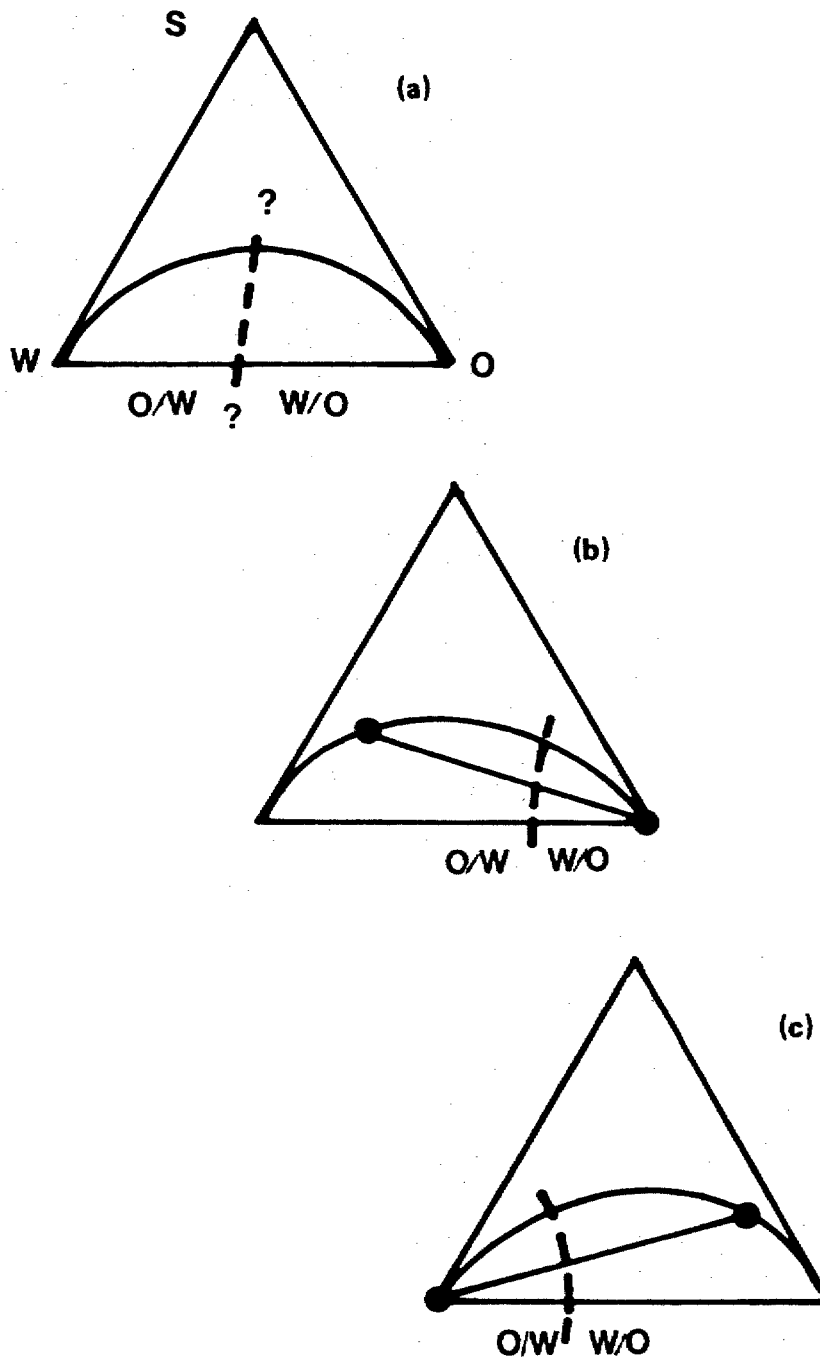


Figure 10. Emulsion type on SOW diagrams.

(a) where is the inversion line? (b) Type I diagram. (c) Type II diagram.

The boundary that separates the two areas is referred to as inversion line. In SOW diagrams consistent with Winsor's types, the inversion line is almost vertical, indicating that the water/oil ratio has a strong influence on the type of emulsion, while the surfactant concentration is of much less importance (Fig. 10a). However, it is worth noting that the surfactant concentration may exert a strong influence on some properties of the emulsion, such as its stability.

Type $\underline{2}$ phase behavior (Fig. 10b) produces O/W emulsions up to typically 70 to 80% oil, whereas type $\bar{2}$ (Fig. 10c) results in W/O emulsion up to about 70 to 80% water. In both cases there is a residual region where the external phase is the one with the highest volume fraction. The exact position of the inversion line depends on the viscosity of both phases and on the emulsification process itself (stirrer, energy input, geometrical shapes). However, the effect of these "physi-cal" parameters is in general either small or well understood [11, 24, 28, 129].

By far the most important effect is due to the nature of the multiphase region, i. e., the type of ternary diagram. Figure 10b and c correspond to Types I and II, $\underline{2}$ and $\bar{2}$ phase behavior, or negative and positive SAD, respectively. It was found that in the central zone of the diagram, i. e., at a water/oil ratio near unity, the type of emulsion is associated with the phase behavior [130-132], that is, to the value of SAD rather than the value of any particular formulation variable. This matches the empirical Bancroft rule [133], according to which "the external phase of the emulsion is the one that contains most of the surfactant," by adding an "at equilibrium" condition for the sake of accuracy. Since the surfactant-rich external phase may solubilize a large proportion of the excess or internal phase, the Bancroft rule may also be stated as: "the external phase is the one which possesses at equilibrium the density nearer to the mean density between the oil and water phase," or "the external phase of a macroemulsion is a micellar solution or a microemulsion, or "the internal phase is the excess phase at equilibrium." These alternative statements of the Bancroft rule will be used below.

The Bancroft rule makes sense when the interactions at the oil/water interface are considered according to the Winsor R approach. Unbalanced interactions result in more solvation or more swelling on one side of the adsorbed surfactant layer, and thus tend to produce a bending of the interface with convexity on the side of the swollen phase, which becomes the external phase. This logical reasoning leads to satisfactory models for microstructures but unfortunately is rather weak when applied to macroemulsions, in which case the drop diameter is too large for the individual surfactant molecule to "feel" the interfacial curvature.

The effect of SAD on emulsion type is found experimentally by carrying out different formulation variable scans at WOR = 1, and determining in each case the type of emulsion obtained by stirring the pre-equilibrated system. Figure 11 shows the variation of the electrolytic conductivity of the emulsion versus formulation for different scans known to modify SAD: salinity of aqueous phase, oil lipophilicity (EACN), surfactant HLB (of a mixture), alcohol content. The emulsion type is readily deduced from the conductivity value since the aqueous phase contains an electrolyte. The conductivity of O/W emulsions is of the same order of magnitude as the conductivity of the W phase (several mS/cm) while the conductivity of W/O emulsions is typically 100- or 1000-fold lower.

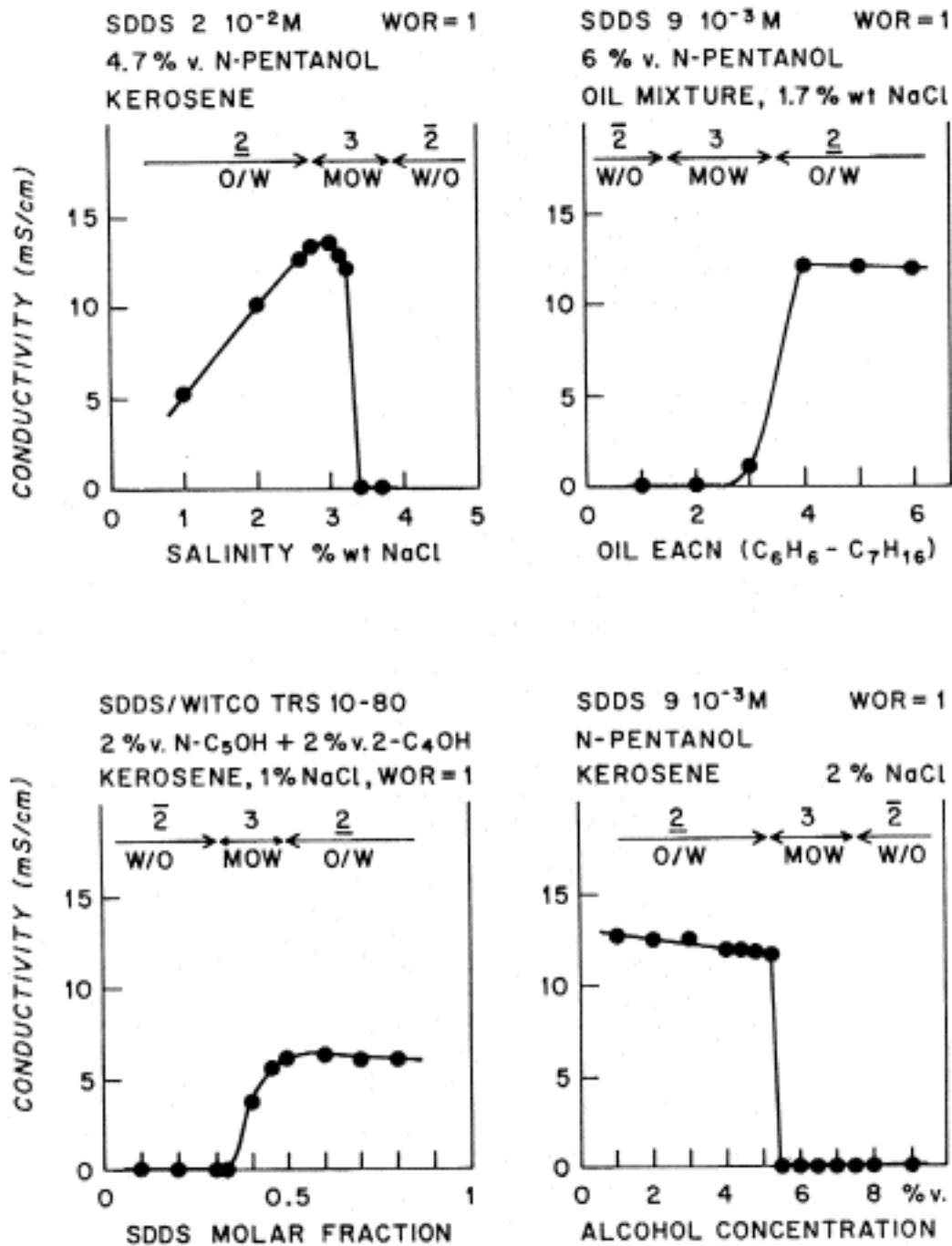


Figure 11. Variation of emulsion conductivity versus formulation for different scans producing a SAD change. (Adapted from Ref. 132.)

In each figure the phase behavior at equilibrium and the emulsion type are indicated. The data show that for all types of scans, the emulsion inversion occurs at or near-optimum formulation for three-phase behavior [132]. In other words, the type of emulsion is associated with the phase behavior at equilibrium.

$$\begin{aligned} \underline{2} \text{ (SAD} < 0) & \quad \text{O/W} \\ 3 \text{ (SAD} = 0) & \quad \text{MOW} \\ \bar{2} \text{ (SAD} > 0) & \quad \text{W/O} \end{aligned} \quad (19)$$

Emulsions obtained in the three-phase range are labeled MOW (microemulsion-oil-water). Figure 11 shows that these MOW three-phase emulsions may exhibit either high or low conductivity, i.e., seem to be water or oil external, depending on the case. Some of the data show that at the crossing of the three-phase zone, the conductivity of the emulsion undergoes a sharp but continuous change. Such a feature tends to indicate that in this type of inversion, there exists in the three-phase range some emulsions with properties intermediate between O/W and W/O. In these systems the surfactant-rich phase is the microemulsion M, the composition of which varies from essentially O to essentially W when the formulation scans the three-phase range referred to as MOW. The conductivity of the M phase changes according to its composition, and it is not unreasonable to think that the microemulsion may be the external phase, with two internal phases. Even more complex possibilities have been suggested [132].

In most commercial applications the surfactant concentration must be kept as low as possible; typical values may vary from 0.1 to 1%. In this range there is no significant effect of the surfactant concentration on the type of emulsion, unless fractionation of a surfactant mixture occurs. Since the tie-line slope of two-phase systems generally increases with surfactant concentration, such an increase tends to strengthen the consequences of the Bancroft rule.

From the previous discussion it is clear that emulsion inversion is essentially due to the effect of two variables: the SAD, which accounts for the combined effect of all formulation variables, and the water/oil ratio or similar quantity, such as water or oil weight or volume fraction.

The actual emulsion type depends on the relative position of the point representing the overall composition of the system in the ternary diagram with respect to the inversion line (see Fig. 10a). Since the surfactant concentration has no significant effect on the inversion position, the use of a ternary diagram provides a surplus of information. Furthermore, the effect of formulation can be observed only by plotting several ternary diagrams, which involves a great deal of experimental work. A more convenient plot than the SOW ternary diagram for studying the emulsion inversion would be one that combines the two most important effects: those of generalized formulation and water/oil ratio or experimental substitutes.

C. Bidimensional Formulation-WOR Diagram

By repeating a formulation scan at different water/oil ratio values, and by measuring the electrolytical conductivity of all emulsified systems, the emulsion type may be mapped on a bidimensional formulation-WOR plot such as that shown in Fig. 12 [134].

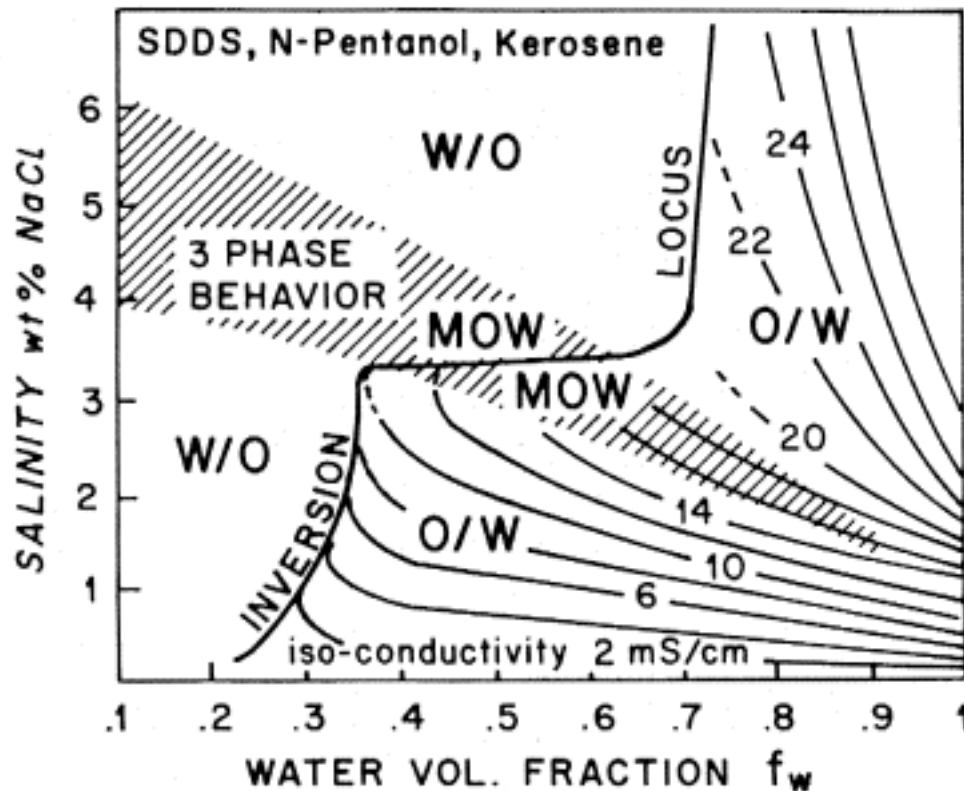


Figure 12. Bidimensional formulation/WOR map showing the phase behavior, the emulsion inversion locus, and isoconductivity contours. (From Ref. 134.)

The ordinate is the salinity of the aqueous phase, i.e., an experimental quantity representing the SAD, since all other formulation variables are held constant. The abscissa is the water volume fraction.

Optimum formulation or zero SAD, in this case optimum salinity, is the centerline of the three-phase behavior band which crosses the diagram from left to right. The slight slope of this line is probably due to a moderate change in surfactant and/or alcohol partitioning with water/oil ratio. Below (respectively, above) the three-phase range, the phase behavior is $\underline{2}$ (respectively, $\bar{2}$).

The isoconductivity curves are drawn for values greater than 1 mS/cm, i.e., for O/W emulsions. All these curves rise slowly from right to left and merge into the asymptote (heavy line), which corresponds to the boundary between O/W and W/O emulsions, i. e., the inversion locus. The slight slope on the isoconductivity curves in the region below the three-phase band is due to the variation of conductivity of O/W emulsions with their external phase content, which is roughly linear. In the upper right zone the much more slanted isoconductivity curves indicate another phenomenon, which is probably the presence of multiple emulsions (see below).

The inversion locus is composed of three branches: first, a central branch located at about unity water/oil ratio, which is roughly horizontal and lies in the three-phase behavior region, then two lateral branches, which are essentially vertical. The lower left one is located in the $\underline{2}$ phase behavior region at about 30% water, while the upper right one lies in the $\bar{2}$ phase behavior region at about 70% water. These two branches match the inversion line position in Fig. 10b and c, respectively.

Such maps have been obtained for a large variety of systems and for all variables capable of altering SAD, including temperature [91, 132, 135-137]. When the water/oil ratio significantly affects surfactant partitioning, the three-phase band may be considerably slanted, but the central branch of the inversion locus still closely follows its trend [134, 137, 138]. Recent work [134,139] tends to indicate that a departure from similar viscosity for O and W phases, as well as a change in energy input during emulsification, might produce a shift in the position of the vertical branches.

Several studies are in progress to understand the quantitative features of such a diagram, but in any case the general inversion phenomenology [134] may be qualitatively rendered by the schematic layout of Fig. 13. The bidimensional map is divided in six regions by the optimum formulation ($SAD = 0$) and the inversion locus lines. Depending on whether the water content of the system is medium, low, or high, the A, B, or C label is used, together with the SAD sign as superscript.

Above the optimum formulation, i.e., for positive SAD, phase behavior at equilibrium is $\bar{2}$, and according to the Bancroft rule a W/O emulsion is expected. When this occurs, as in the A+ and B+ regions, a "normal" medium or low internal phase ratio W/O emulsion is obtained. In the C+ region the phase behavior ($\bar{2}$) and the Bancroft rule would predict a W/O emulsion, but the amount of oil is too low to make it the external phase, and the resulting dispersed system is an "abnormal" O/W emulsion. As may be deduced from the data of Fig. 12, the conductivity of such C+ O/W emulsion is somewhat lower than would be expected from its water phase salinity and content; experimental evidence indicates that C+ abnormal emulsions are often multiple ones of the W/O/W type, which is, as a matter of fact, a way for the system to partially satisfy the Bancroft rule. Below the optimum formulation, i. e., for negative SAD, the opposite equivalent phenomenology is found, with normal A- medium and C- low internal phase ratio O/W emulsions, and abnormal B- W/O emulsions.

The usefulness of the SAD-water/oil ratio plot is enhanced by the fact that it matches the mapping of the emulsion properties [140,141]. The isostability curves are found to fit closely the six region's boundaries. Normal emulsions either in the A+B+ (W/O) or A-C- (O/W) regions are found to be relatively stable, with increasing stability at constant SAD when approaching the A+/C+ or A-/B- limit, i. e., with increasing internal phase ratio; at constant water/oil ratio in the central region, stability decreases rapidly from both sides when approaching the A+/A boundary.

However, the previously described phenomenology deals with the properties of emulsions obtained by stirring pre-equilibrated SOW systems. For most of the processes of practical interest the inclusion of an equilibration lag time may not be feasible, and as a matter of fact, some of these processes must handle systems which are already emulsified. It is thus necessary to examine how this phenomenology is modified when SAD and/or the water/oil ratio are changed in an existing emulsion, i. e., in nonequilibrium processes, from the physicochemical point of view.

D. Apparent Equilibration Time and Dynamic Inversion

Two significant nonequilibrium phenomena have been dealt with in recent investigations. The first concerns the determination of the minimum contact time between phases of a SOW system to reach such a state that the corresponding emulsion type and properties are indiscernible from those of an emulsion prepared by stirring an equilibrated system of identical composition and formulation. The studies [149,150] were carried out under the most adverse conditions, i.e. , when the surfactant is initially dissolved in the phase which is to be the excess phase at equilibrium; as a consequence, most of the surfactant ought to migrate by diffusion from one phase to another during the equilibration process. The contact time beyond which a partially equilibrated system produces upon stirring the same type of emulsion as a completely equilibrated system of the same formulation and composition is referred to as the *apparent equilibration time*. The main conclusion of these studies is that the apparent equilibration time decreases when SAD approaches zero, and that it is essentially zero for some near optimum formulation systems. This result tends to indicate that the phenomenology discussed previously is probably valid for nonequilibrium systems located not too far from the optimum formulation.

The second type of study [151,152] tried to mimic actual processes by starting with an emulsion and shifting the position of its representative point on the formulation-water/oil ratio map by means of a change of one of these variables. SAD may be changed without significant alteration of the water/oil ratio, for example by modifying the temperature or by adding a small amount of concentrated chemical solution, such as in the injection of demulsifier in crude dehydration. The water/oil ratio may be changed at constant SAD, such as in mayonnaise manufacture, by adding to the stirred emulsion increasing amounts of internal phase. The water/oil ratio may be varied not only in time but also in space by using special emulsifying devices capable of mixing action only over a part of the whole system, such that the volume actually stirred might possess a different water/ oil ratio [153].

When the result of one of the above-mentioned changes is to shift the representative point of the system to the other side of the inversion locus, a so-called *dynamic inversion* of the emulsion takes place. The experimental evidence reported elsewhere [151,152] is illustrated by Fig. 14.

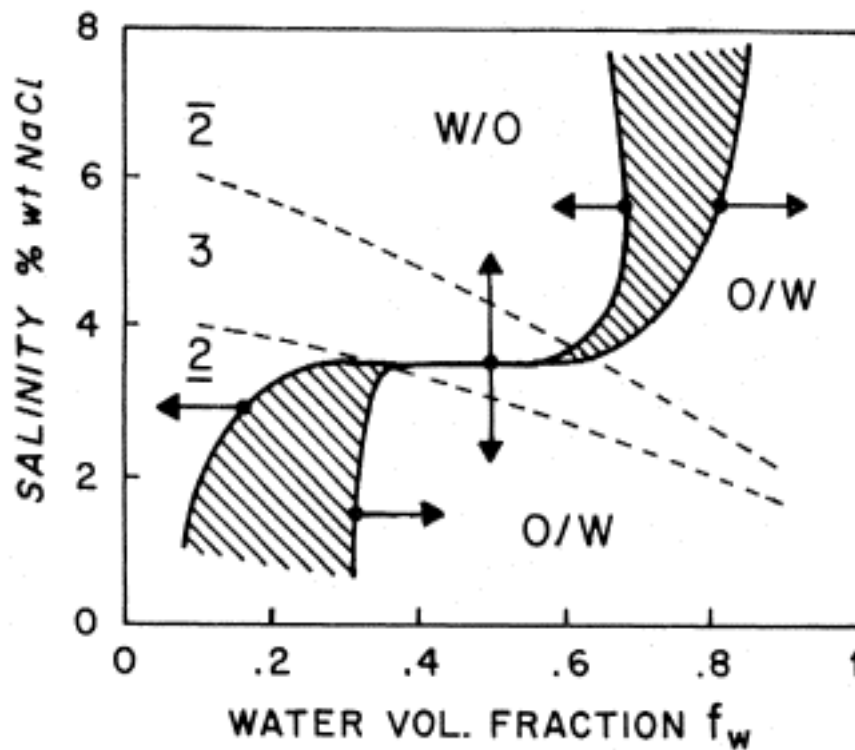


Figure 14. Dynamic inversion locus showing the hysteresis zones (shaded). Arrows indicate the direction of change. (Adapted from Ref. 151.)

In these experiments, an equilibrated SOW system, whose formulation and WOR correspond to a position near the inversion locus for pre-equilibrated system (Fig. 12), is emulsified. This initial emulsion is maintained under permanent stirring and its formulation or WOR is modified such that the representative point on the bidimensional plot moves toward and beyond the inversion locus. The electrolytic conductivity is monitored to detect the emulsion inversion. The arrows in Fig. 14 indicate the direction of change of WOR or formulation for each inversion line.

The dynamic inversion due to a SAD change through the A+/A- boundary i. e., the central horizontal branch, occurs at the same position whatever the direction of change of SAD. Other experimental evidence indicates that this first type of inversion, so-called *transitional* is reversible and that it is essentially the same as that obtained with emulsions obtained from pre-equilibrated systems.

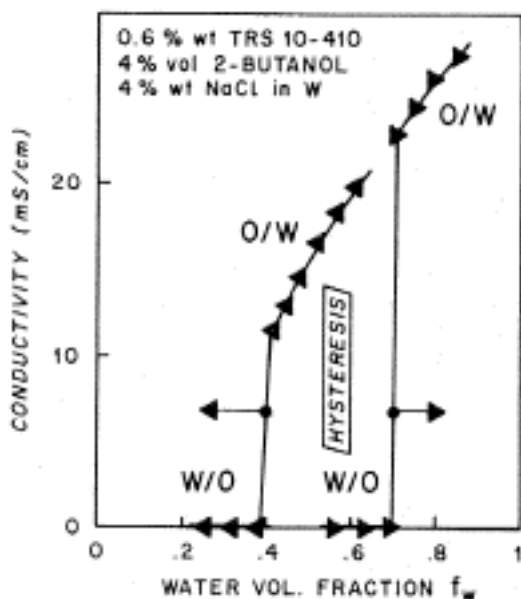


Figure 15. Variation of the emulsion conductivity through a dynamic inversion produced by an increase in internal phase ratio.

Arrows indicate the direction of change. (From Ref. 151.)

On the other hand, the *dynamic* inversion due to a change in water/oil ratio produced by addition, upon stirring, of a certain amount of one of the phases to the pre-existing emulsion shows quite different features. Indeed, the inversion of the emulsion does not occur at the same water/oil ratio, depending on whether the WOR is increasing or decreasing. Figure 15 shows the variation of conductivity of the W/O emulsion (A+) when the W phase content is increased (arrows pointing to the right), and the same data for the O/W emulsion (C+) when the O phase content is increased (arrows pointing to the left). Obviously, the emulsion inversion does not occur at the same WOR value. Instead, this second type of dynamic inversion exhibits a *hysteresis* zone [128], i. e., a region of the map in which the emulsion may be either O/W or W/O, depending on its previous history. Figure 14 shows that a wedge-shaped zone (shaded area) replaces each of the A+/C+ and A-/B- branches of the inversion locus. Hysteresis is linked with irreversible instability phenomena, sometimes referred to as catastrophes. From this characteristic, this second type of dynamic inversion is denoted *catastrophic*. As seen in Fig. 14, the hysteresis zones of catastrophic inversion vanish at the optimum formulation, i. e., at zero SAD, where the transitional inversion takes place.

Any satisfactory interpretation of such complex phenomena must include the main features of the two types of emulsion inversion and link them with the various cases of phase behavior.

III. Thermodynamic Modeling of Discontinuous Phenomena

A. Thermodynamic Approach to Emulsion Inversion

From the thermodynamic point of view macroemulsions are unstable since ultimately they must end as a coalesced system. During the breaking process, the interfacial area decreases, and as a consequence so does the free energy of the system. However, this coalescence process is slow with respect to what may be called the kinetics of inversion, with the exception of near-optimum formulation systems. From the experimental data and the discussion in Sec. II it is clear that emulsion inversion is closely associated with the thermodynamics framework of phase behavior at equilibrium. A thermodynamic approach to emulsion inversion was recently suggested by Dickinson [154] on the premise that an emulsion is formed by a spinodal decomposition of a molecular mixture of the components similar to the phase splitting of metal alloys upon cooling [155-159]. The idea is attractive because it links the phase separation process, which takes place in order to reduce the free energy of the system, with the occurrence of the emulsion. Furthermore, the effect of the interactions at the interface may be important at the very start of the seeding process and thus may control the emulsion type. However, the entire scheme does not match the experimental facts; the facts match only in the neighborhood of a critical point. The model discussed here is based on simple free energy considerations and assumes that the emulsion type depends on a free energy potential and that a possible state occurs at each potential minimum.

It is known that a system with roughly similar amounts of O and W phases can be emulsified either as a O/W or W/O emulsion. According to Sec. II, one type is favored over the other by the nature of the formulation. However, the opposite type may often be obtained by experimental tricks, such as the addition of one of the phases little by little upon stirring, i. e., the production of local conditions quite different from the overall or final ones. This possibility implies that the free energy function of the emulsion must have two minima, i. e., two possible states. The change from one of these states to the other, namely the emulsion inversion, would require a free energy input sufficient to jump over the potential maximum or barrier which separates the states. The analogy of a ball in a hole (Fig. 23) may be useful in understanding these concepts but is insufficient to carry out an analysis. In order to describe and interpret these discontinuous changes a special mathematical tool must be used, for example the framework of catastrophe theory.

B. Catastrophe Theory Basics

Starting from algebraic topology, Thom laid the basis of catastrophe theory and demonstrated the importance of the concept of structural stability [160], i. e., the insensitivity of a system to small perturbations about a minimum energy state. He showed that discontinuities in the behavior of natural phenomena might be interpreted, at least locally, by means of one of the seven elementary catastrophe models. In the past 10 years, catastrophe theory has slipped out of the hands of the mathematicians to become

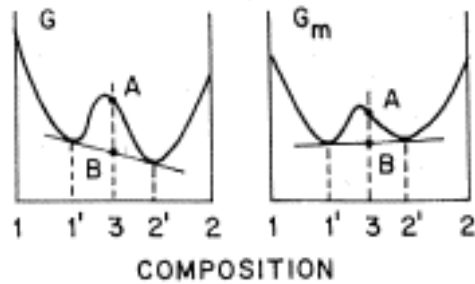


Figure 16. Gibbs free energy and mixing free energy versus composition of a binary, showing phase splitting.

a useful tool for scientists and engineers, who have used it to interpret scores of physical and thermodynamic phenomena [161-163].

In spite of the complexity of its topological foundation, the catastrophe theory framework is rather simple to use. The typical approach is to start with the selection of a potential which is a function of two types of variables: the state and control variables. When symmetry considerations do not compel the contrary, the state variable is taken as unidimensional [163]; this variable describes an intrinsic property of the system, such as phase density or interface curvature. As in state space analysis of control systems, it is not necessary to attain an experimental determination of this variable; however, it is important to have at least an intuitive grasp of its meaning. Control variables are observable and can be manipulated; they match the role of ordinary variables, such as temperature, pressure, composition, or formulation.

To clarify these concepts, catastrophe theory will be applied to the interpretation of a well-known phenomenon, i.e., the phase splitting of a binary (1-2) system. The classical thermodynamic treatment deals with the variation of the Gibbs free energy of the system versus composition, at constant temperature and pressure [164]. The phase rule indicates that there may be up to two phases at equilibrium; hence the Gibbs free energy should exhibit up to two minima. Figure 16 shows a typical variation of the Gibbs free energy and of the excess or mixing free energy versus the composition variable. For a composition identified by number 3, the one-phase system (A) would have a higher free energy than the two-phase system (B), which corresponds to a splitting into phase 1' and 2'.

The instability of the one-phase system arises from the existence of a maximum in the free energy. The region limited by the two inflection points on both sides of the maximum is the spinodal decomposition zone. In mathematical terms, this zone is characterized by a downward concavity:

$$\frac{\partial^2 G}{\partial X^2} \Big|_{T,P} < 0 \quad (20)$$

The boundary between stability and instability when the G function is affected by some external variable, such as temperature or the addition of a third component, is called the marginal stability and corresponds to the case in which the inflection tangent is horizontal, i.e.



Figure 17. Variation of the free energy graph in the case of a 2 → 1 phase transition at a bicritical point. (From Ref. 110.)

$$\frac{G}{x} = 0 \quad \text{and} \quad \frac{\partial^2 G}{\partial x^2} = 0 \quad (21)$$

The concept of marginal stability is important because it is associated with the phase behavior transition of the binary system. Marginal stability may occur by reason of two types of modification of the free energy potential by an external variable such as temperature or the addition of a third component [110].

The first type of modification is illustrated in Fig. 17, in which the two existing minima merge and squeeze the maximum between them. In this case three extrema (crosses) merge together and the resulting minimum is of third order, i. e., the three first derivatives are zero at that point. From the physical point of view, the compositions of the two phases in equilibrium get closer and closer and finally become indiscernible at a critical point. To be more accurate, such a point should be called bicritical since it corresponds to the merging of two phases.

The second type of marginal stability is illustrated in Fig. 18, where one of the two minima merges with the maximum, while the other minimum remains separate. At this point, called monocritical, two extrema are merging and the two first derivatives are zero. From the physical point of view, this point matches the disappearance of one phase by solubilization in the other with no (ordinary) critical point.

If the external variable that produces the change is, for example, the surfactant concentration added to a O-W binary, the bicritical transition corresponds to the crossing of the binodal curve at the plait point where the tie line becomes tangent, while the monocritical transition corresponds to crossing of the binodal curve at any other point.



Figure 18. Variation of the free energy graph in the case of a 2 → 1 phase transition at a monocritical point. (From Ref. 110.)

It is now time to select one of the seven elementary catastrophes, described by Thom, to fit the case studied. Since the free energy potential must exhibit up to two minima and a maximum, i.e., three extrema, the fourth-degree polynomial of the second or "cusp" catastrophe is selected:

$$G_{cd}(x) = \frac{x^4}{4} + \frac{c x^2}{2} + d x \quad (22)$$

where x is the state variable, and c and d are the control variables. This expression of a fourth-degree potential is quite general, since any third-degree term may be eliminated by a proper change of variable x , and since the eventual constant term may be taken as the zero reference of the potential.

Thus two control variables c and d appear naturally from the model as the coefficients of the second- and first-degree terms. Fractional coefficients are used for the sake of simplicity and are also not limiting in any way.

A potential extremum (maximum or minimum) is obtained whenever the first derivative of G is zero.

$$\frac{\partial G}{\partial x} = x^3 + c x + d = 0 \quad (23)$$

Solution of this third-degree equation would result in up to three roots, i. e., three extrema, as sought when this potential expression was selected. Equation (23) may be expressed as a function $x(c,d)$ which represents a surface, called a *manifold*, in a (x,c,d) space (see Fig. 19). The manifold is the geometrical locus of G extrema. This cusp manifold exhibits a wedgelike fold. For each set of (c,d) control variables a vertical line crosses the manifold; each crossing corresponds to the x value for a G extremum, as indicated in

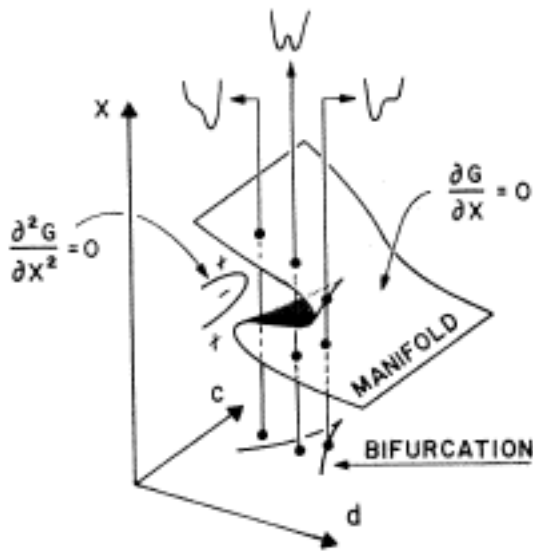


Figure 19. Manifold and bifurcation of the cusp catastrophe.

Fig. 19 by the $G(x)$ illustrations (top of Figure). The upper part of the manifold corresponds to a G minimum at high x , i.e., on the right side in the $G(x)$ illustration, and conversely. The central crossing of the fold corresponds to a G maximum and matches the region where the second derivative is negative. The points of interest on this surface are those in which the number of extrema changes, i.e., the mono- and bicritical point singularities [163]. At such points the second derivative of G is also zero:

$$\frac{\partial^2 G}{\partial x^2} = 3x^2 + c = 0 \quad (24)$$

One such point is shown in Fig. 19, for which the vertical line is tangent to the fold and the corresponding $G(X)$ curve exhibits a horizontal inflection point. Equation (24) is plotted on the (x,c) plane and corresponds to the projection of the line of tangency of the vertical lines with the fold.

By eliminating x between Eqs. (23) and (24) the projection of the locus of critical points on the (c,d) subspace is obtained. This projection the so-called **bifurcation**, is expressed in this case by the following relationship, which is cusp shaped:

$$B(c,d) = \frac{d^2}{2} - \frac{c^3}{3} = 0 \quad (25)$$

For values of c and d belonging to the inside of the cusp, G possesses two minima, while it has only one exterior to the cusp. For c and d corresponding to Eq. (25), i. e., for the bifurcation, G exhibits one minimum and another point with a horizontal inflection tangent which indicates marginal stability at a monocritical. point. At the apex of the cusp ($c = 0, d = 0$) there is a bicritical point (see Figs. 17 and 18).

Coming back to the case of a O-W binary change with a third variable such as surfactant concentration, Fig. 20 shows the analogy between the SOW diagram and the bifurcation of the cusp catastrophe. Control variable d matches the role of the composition of the O-W binary, i.e., the water/ oil ratio, while control variable c corresponds to the effect of surfactant concentration. The cusp line represents the binodal curve, and the apex of the cusp corresponds to the plait point of the binodal curve.

The $G(x)$ curves of Fig. 20 (left illustration) allows a complete understanding of the analogy when the x value at a G minimum is associated with the composition, i.e., oil phase at low x and water phase at high x . When there is a single minimum of G at high x , i.e., on the right, it represents a W phase, and conversely. When crossing the left branch of the cusp from outside to inside, a second minimum appears at low x and represents an incipient O phase.

C. Conventions

Before proceeding further in the use of the bifurcation of the cusp catastrophe to interpret the phase behavior of a SOW ternary, it is necessary to examine the two types of convention employed in discussions-of catastrophe theory [163].

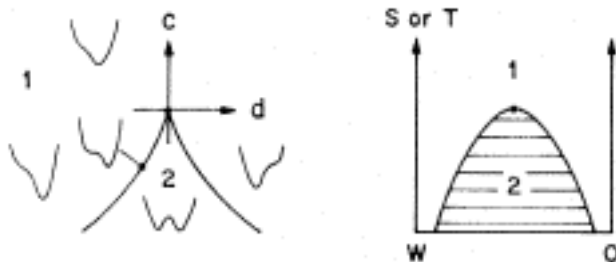


Figure 20. Interpretation of the phase behavior of a W-O binary versus surfactant concentration or temperature.

In the previous example the analogy implies that whenever G exhibits two minima, as inside the cusp or below the binodal curve, the system splits into two phases, whose compositions are defined as in Fig. 16. If x does not represent the O-W binary composition for this value of S , but rather a structural variable such as phase density in the ternary diagram, it may only be said that the system splits into two phases, whose characteristics are located near the G minima. The exact composition of these phases depends on a mass balance and requires the accurate definition of state variable x . This is not necessary for the present qualitative interpretation. The important fact is that if G has two minima, the system spontaneously splits into two phases in order to decrease its total free-energy. When G has several minima, this so-called *Maxwell convention* compels the system to fractionate into several parts, each corresponding to a possible state, i.e., a G minimum, so that the overall G function of the system is minimized.

When applied to the phase behavior of ternary systems, this corresponds to tie-line splitting between two phases or tie-triangle decomposition into three phases. In order to take into account this Maxwell convention in the previous cusp example, the doubling of the manifold surface should be truncated along the locus of critical points in the (c,d) space, i.e., Eq. (25), and replaced by a tie-line surface such as in Fig. 21. The upper part of the manifold at low values of d , say more W than O, exhibits a one-phase system of high density, i.e., a water-based microemulsion. The opposite applies for the lower part of the manifold. Figure 21 indicates the shape of the $G(x)$ free energy at a point located inside the cusp and at the two ends of the corresponding tie line where monocritical behavior occurs. The $G(x)$ curve is also illustrated at the bicritical plait point.

The Maxwell convention is, however, not the only one to be used in catastrophe theory discussions. For certain applications, such as emulsion type interpretation, only one state may exist at a given time, i.e., O/W or W/O, in spite of the eventual coexistence of several possible states, i.e., minima of G . The actual state of the system would be one of the possible states, specifically the one that is favored by the previous history of the system. In such a case the system remains in its original state until this state disappears. This occurs when the corresponding G minimum vanishes as a consequence of the effect on some change in the control space. This second case is referred to as the *perfect-delay convention*.

D. Application of the Cusp Catastrophe to Emulsions

The case considered is still that of a O-W binary, to which a third component is added to reduce the range of immiscibility. Let us now assume that the cusp catastrophe potential may represent the free energy of the emulsified system. As pointed out by Dickinson [165], this makes sense because emulsions are single-state systems, either O/W or W/O, and they exhibit inversion hysteresis. It is assumed that in this interpretation, the state variable x stands for the density of the external phase of the emulsion; if x is higher (respectively lower) than the average density between O and W, the emulsion is of the O/W type (respectively, W/O). The reader well versed in interfacial physical chemistry may consider x as the curvature of the interface, taken as positive when the concavity is toward the oil phase [165]. This second meaning of x embodies a more structural information content, but does not enhance the discussion. For the sake of simplicity, it is convenient to adhere to the first meaning of x , i.e., the density of the external phase expressed as the deviation from the average density of O and W. In the present case of a single-state system, the perfect-delay convention is the compulsory choice. It will become apparent that c and d control variables have the same meaning as previously.

The manifold and the bifurcation are, of course, the same as in the phase behavior interpretation, but with a different meaning (see Fig. 22). Outside the cusp, there exists only one G minimum and one possible type of emulsion, which is O/W at high x and W/O at low x . The control variable d matches the effect of the water/oil ratio; in order to fit the experimental data, a high d value (respectively, low) should correspond to a high (respectively, low) oil content of the external phase. This also represents the meaning of d in the phase behavior interpretation.

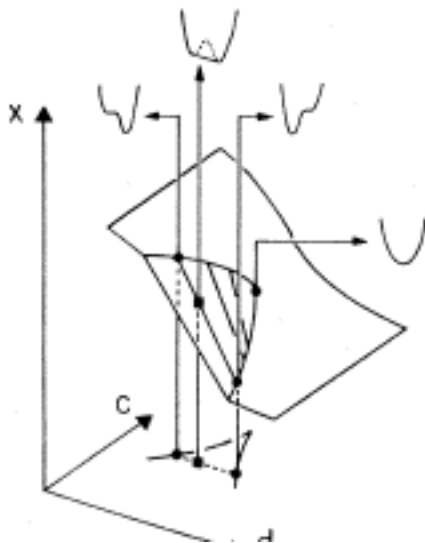


Figure 21. Manifold of the cusp catastrophe with the fold truncated and replaced by a tie-line surface according to a Maxwell convention.

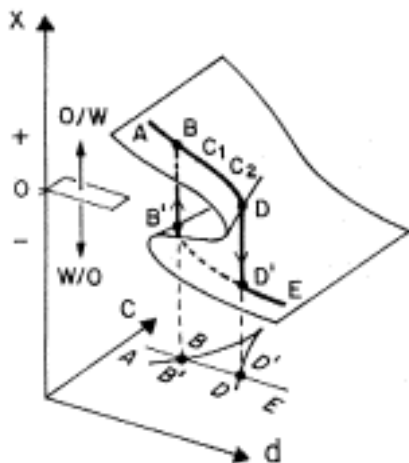


Figure 22. Interpretation of emulsion inversion by a cusp catastrophe model according to a perfect-delay convention.

Inside the cusp the emulsion may be either O/W or W/O, i.e., may respectively correspond to the higher or lower part of the fold, depending on the memory feature of the perfect-delay convention. It is worth remarking that the central part of the fold does not represent a minimum but a maximum of G , i.e., no state corresponds to it. As a matter of fact, this part of the manifold (which corresponds to a G maximum) can be cut out along the critical point locus with no loss of information.

In order to understand the role of the perfect-delay convention, let us suppose that a O/W emulsion (high x , low d) is altered by adding increasing amounts of oil (increasing d) without changing surfactant concentration. The system would follow a constant c trajectory in the direction of increasing d , which is indicated as path ABCDE in Fig. 22. Point A lies in the single-state region corresponding to O/W emulsions; thus the original emulsion is O/W. When the trajectory crosses the two-state region at B, the emulsion remains O/W according to the perfect-delay convention, and it does so from B to D.

In geometrical terms the representative point of the emulsion state stays on the upper-part of the fold. At D the path exits the two-state region and the O/W state, i.e., the G minimum at high x , disappears. As a consequence, and according to the perfect-delay convention, the emulsion is compelled to change state, i.e., to invert to a W/O emulsion, which is the only possible state for the remaining trajectory D'E. When this change is followed on the manifold figure, it is clear that the inversion corresponds to a jump from the upper part, point D (high x , O/W), to the lower part, point D' (low x , W/O). This interpretation corresponds to the catastrophic character of emulsion inversion by a change of water/oil ratio [128,165].

Let us suppose that the starting point is E, which corresponds to a W/O emulsion, and that the previous path is followed in the opposite direction from E to A by decreasing d , i.e., increasing the water content of the emulsion. When the trajectory enters the two - state region at D', the emulsion remains W/O according to the perfect - delay

convention, and so goes from D' to B' . When B' is reached the W/O state disappears, and the system must change to O/W at B . The latter state is maintained over the BA part of the trajectory. In this second direction of change the inversion, i.e., the jump, occurs at $B'-B$, that is, for a d value different from that of the previous case.

Figure 23 illustrates what happens during the two anterior changes with a *ball-in-a-hole analogy*. The black dot represents a ball and stands in the current minimum energy state of the system. The hole of potential energy has the shape of the $G(x)$ function, and the crossing point of the axes refers to zero x , i.e., a density of the external phase intermediate between those of O and W. When the ball is in a negative x (left) hole the emulsion is W/O, and conversely. Figure 23 also illustrates the test tube appearance of the emulsion in each case, with the oil and water phases represented as black and white, respectively.

The inside of the cusp, i.e., segment BD in this example, corresponds to the hysteresis zone in which inversion is delayed until the disappearance of the occupied state forces the ball to fall in the other hole. Depending on its previous history, the emulsion may be either O/W or W/O for (c,d) values corresponding to the inside of the cusp, i.e., the hysteresis zone. Such an analogy makes it clear why this type of inversion is irreversible and why it has earned the designation "catastrophic". Indeed, both the G and x values suffer a discrete jump.

This analogy allows the prediction of what may happen if the ball does not stay quietly in its position, but is permitted to fluctuate slightly about it, as in actual systems submitted to small perturbations. In such a case the jump of the ball may occur whenever the energy barrier between the actual and prospective states, i.e., the intermediate G maximum, is low enough with respect to the current position, or whenever the x distance between minimum and maximum is short. The consequence is that the change will happen before the trajectory exits the two-state region, so that the hysteresis zone will shrink. This may be regarded as a nonperfectly delayed inversion, and should correspond

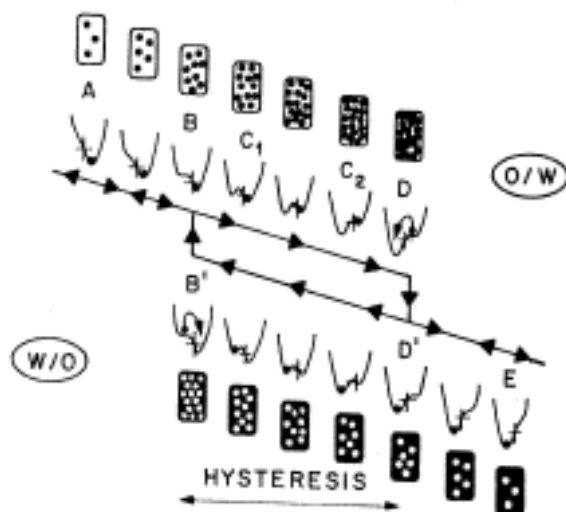


Figure 23. Ball-in-the-hole analogy to interpret the emulsion inversion features by means of the cusp bifurcation. (Adapted from Ref. 166.)

to most actual emulsion systems. In the extreme case of emulsification of pre-equilibrated systems, the emulsion has no previous state, thus no memory phenomenon may apply, and the limit between O/W and W/O regions is a single line. The position of this line would depend on the $G(x)$ shape, according to the Bancroft rule stated in Sec. II.B, and would lie probably somewhere in the middle of the perfect-delay hysteresis zone. This is just what the experimental evidence shows (see Sec. II.D).

E. Insufficiency of the Cusp Model

This cusp catastrophe model has the advantage of simplicity, and other information may be obtained from it [165]. However, it has the serious drawback of being symmetrical with respect to the control variable d , which represents the water/oil ratio effect. In fact, it is known that real two-phase systems do not exhibit such a symmetry, as may readily be deduced from the slanting of the tie lines and the side position of the plait point on the binodal curve. As a consequence, the cusp model cannot handle the difference between type I and type II diagrams and their associated phase behavior and emulsion type. Furthermore, the potential function of the cusp catastrophe is of fourth degree only, and thus exhibits at most two minima, i.e., two states. In order to render the occurrence of a three-phase system, a higher-degree potential function would have to be used.

Beyond its use as an introductory example, however, this cusp catastrophe model shows that both phase behavior and emulsion inversion may be interpreted by means of the same potential and the same control variables [166]. Indeed, the only divergences are the compulsory ones inherent in the different natures of the two problems, i.e., the significance of x and the proper convention.

In spite of the fact that both interpretations deal with an O-W binary to which a third component S is added to reduce the two-state zone, the similarity is somewhat surprising. Indeed, the phase behavior transition is a thermodynamic phenomenon which occurs reversibly at equilibrium, while the emulsion inversion is an irreversible process of quite different nature, at least intuitively. The fact that they may be interpreted by the same model enhances Dickinson's claim of the hidden thermodynamic character of emulsion formation and inversion [154].

IV. Surfactant /Oil /Water Ternary Systems

A. Selection of a Catastrophe Theory Model

SOW ternary systems of the Winsor types may exhibit up to three phases at equilibrium. In such ternaries there exist two types of two-phase emulsion, i.e., O/W and W/O, and one type of three-phase emulsion, referred to as MOW (see Sec. 11). In both cases, the interpretation requires up to three states. Thus, the free energy potential should exhibit up to three minima. Since the composition of a ternary diagram is defined by two independent variables, the extension of the case of Fig. 16 would lead to a tridimensional representation of the free energy versus two composition variables [167]. The tangent line in Fig. 1.6 would be replaced by a tangent plane, and so forth. Such a representation gives a fair account of the phase behavior of a specific type of diagram. However it is

quite difficult to show the effect of the formulation variables with it, and there is still much work to be done to develop a complete model on this basis.

Because of the intrinsic and structural character of the state variable x used previously, there is no need to make it bidimensional. As seen in Sec. II and III the phase density information is sufficient to describe the effects inside and at the boundaries of the multiphase region. Moreover, in the previous example the composition effects are taken into account by the control variables c and d .

If the model G function is required to exhibit up to three minima, the corresponding polynomial of a single state variable should be of the sixth degree, so that its derivative might have up to five roots, i.e., three minima and two maxima. These conditions match the fourth elementary catastrophe, the so-called *butterfly*, after the shape of its bifurcation [163]. Its polynomial potential in its most reduced form may be written as

$$G_{abcd}(x) = \frac{x^6}{6} + \frac{a x^4}{4} + \frac{b x^3}{3} + \frac{c x^2}{2} + d x \quad (26)$$

The lack of fifth-degree and constant terms is not limiting, since the former may be eliminated by a proper change of variable x , and the latter may be taken as the zero reference of the potential. Thus, four control variables arise naturally from this expression. Their meaning will be discussed later, but it may be seen at once that this potential shares some properties with the cusp in specific cases. For example, for $b = 0$ and $a = 0$ the two expressions will lead to the same topological results, resulting in equivalent behavior. This gives a hint that c and d will have the same meaning as in the cusp catastrophe model. Since the only odd terms are those of the first and third degree, a change from x to $-x$ may be compensated by a change of sign of both b and d ; this means that $(b=0, d=0)$ is a center of symmetry of the problem.

The equation of the manifold, i.e., the geometrical locus of G extrema, is

$$\frac{G}{x} = x^5 + a x^3 + b x^2 + c x + d = 0 \quad (27)$$

At the singularities of this manifold, i.e., at critical points,

$$\frac{{}^2G}{x^2} = 5 x^4 + 3 a x^2 + 2 b x + c = 0 \quad (28)$$

By eliminating x between Eqs. (27) and (28) the bifurcation is obtained:

$$B(a,b,c,d) = 0 \quad (29)$$

In the present case the representation of the manifold as $x(a,b,c,d)$, and of the bifurcation, require five and four dimensions, respectively, which is too many to handle in a general way. However, it is worth noting that since the bifurcation indicates the relative position of the different critical points in the control space, it is of first importance to establish its graphical representation in order to compare it with the corresponding experimental data, as was done for the cusp model.

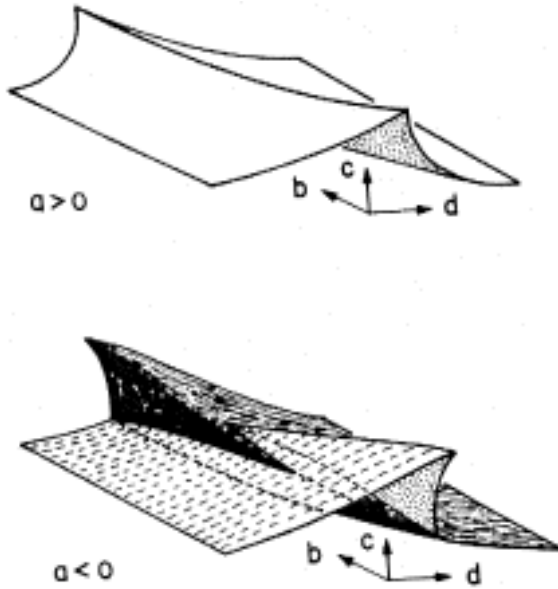


Figure 24. Three-dimensional (b,c,d) cut of the bifurcation of the butterfly catastrophe for $a > 0$ and $a < 0$.

Figure 24 shows the (b,c,d) representation of the butterfly bifurcation in two typical cases, i.e., for positive and negative values of control variable a . When a is positive the bifurcation is no more than the three dimensional extension of the cusp case, with b acting as a symmetry breaking variable. When a is negative the self-intersecting surface has an odd shape which is too complex to discuss conveniently.

As seen in Secs. I and II, the plots of interest, i.e., the SOW ternary phase behavior diagram and the formulation-WOR inversion map, are both bidimensional. Hence the study of the features of the butterfly catastrophe may be carried out conveniently using bidimensional sections of the control space, e.g., plane cuts in Fig. 24.

B. Interpretation of the Phase Behavior of SOW Ternaries

1. Winsor Type I or II Ternary Diagrams

To obtain a bidimensional cut of the control space, two of the four control variables must be held constant. In the cusp model it was seen that the coefficients of the first- and second-degree terms corresponded to the role of water/oil ratio and surfactant concentration. Hence, the effects of variables c and d will be studied first, by fixing the values of both a and b .

For $a = 0$ and $b = 0$, the (x,c,d) manifold and the (c,d) bifurcation cuts are essentially those of the cusp catastrophe, except that the apex of the cusp is of higher order and corresponds to a tricritical point. The interpretations of the preceding section fully apply to this case. As far as the phase behavior is concerned, this means that c and d match the role of the surfactant concentration and the water/oil ratio, for a SOW ternary diagram with a plait point in the center of the diagram ($d = 0$); positive d corresponds to more oil than water, and conversely. When keeping $b = 0$, the increase of a from zero does not

affect the general aspect of both the manifold and the bifurcation. Increasing a results only in a more acute cusp, and the restoration of the apex as a bicritical point.

The change of the (c,d) bifurcation with b for $a \geq 0$ is easily deduced from Fig. 24 by shifting a cut of plane (c, d) along the b axis. Figure 25 shows that when b departs from zero, the bifurcation keeps its cusp shape but loses its symmetry with respect to d . The apex of the cusp is displaced to positive (respectively negative) values of d when b is positive (respectively, negative). Hence the plait point of the matching SOW diagram is shifted similarly. This means that the $b > 0$ case may represent a Winsor Type I diagram, while the $b < 0$ fits a Type II diagram. This is the first indication that b corresponds to the effect of formulation as expressed by the negative value of SAD. However, for these positive values of a , the intermediate Type III diagram is not found, but instead, a diagram with a diphasic zone showing horizontal tie lines.

2. Winsor Type III Diagram

It is seen from Fig. 24 that when a is negative, the bifurcation has a much more complex geometry. If b does render the actual effect of negative of SAD, a Type III diagram should be sought at $b = 0$. Figure 26 shows the aspect of the $x(c,d)$ manifold for $a = -10$ and $b = 0$. In order to improve the representation, the space has been split at constant c and the cut has been opened. This allows us to visualize a good perspective of both the high and low c portions of the manifold. This surface presents, at high c , two overlapping folds which result in a bifurcation (c,d) cut composed of two intersecting cusps, from which the denomination butterfly comes. The splitting of Fig. 26 has been done for the c value that corresponds to the complete overlapping of the two cusps. At lower c values the two cusps merge into a single fold when the residual overlapping region vanishes as an inverted cusp. The vertical lines correspond to different (c,d) values for which the manifold is intersected an odd number of times. Each intersection represents an extremum of G , i.e., a minimum or a maximum depending on the sign of the second derivative, plotted as Eq. (28) on the (x,c) plane. Above each vertical line, a graph shows the shape of the $G(x)$ potential for the particular (c,d) set of values. The position of each minimum with respect to $x = 0$ indicates the nature of the phase represented [168]. If x is positive (upper fold crossing) it is a W phase, while if x is negative (lower fold crossing) it is an O

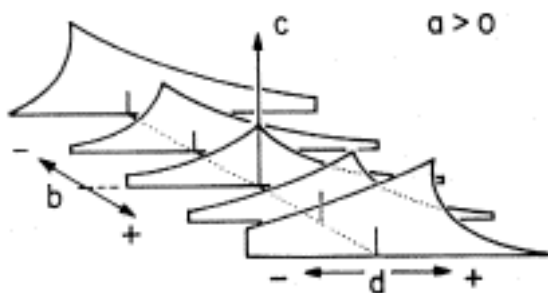


Figure 25. Sections at constant b of the butterfly catastrophe bifurcation for $a > 0$.

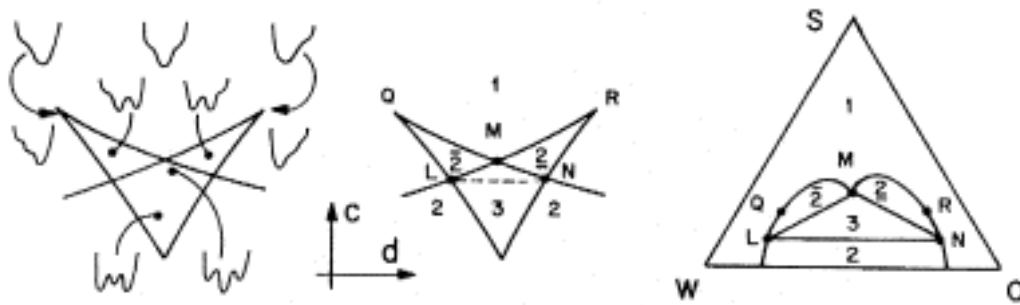


Figure 27. Interpretation of the phase behavior on the butterfly catastrophe bifurcation (c,d) cut and on matching Winsor type III diagram for $a < 0$ and $b = 0$. (From Refs. 166 and 168.)

Figure 28 shows a water/oil ratio scan at a constant surfactant concentration corresponding to three-phase occurrence. The $G(x)$ aspect is drawn for several points inside and at the boundaries of the different regions, which are crossed by the A-I path. A is a micellar solution with a high content of W ($x \gg 0$). At B a horizontal inflection tangent point for near zero- x indicates the incipient occurrence of a microemulsion, which is in equilibrium with a W excess phase at point C ($\bar{2}$). When point D is reached the horizontal inflection tangent point at $x \ll 0$ marks the beginning of the occurrence of an O excess phase. At E the three minima of G fit the three-phase behavior. At point F the minimum corresponding to the W phase vanishes, and a two-phase type $\bar{2}$ is obtained at G. Changes from F to I are symmetrical to D-A ones with respect to d , i.e., exchanging the roles of O and W.

If such a left-to-right water/oil ratio scan were carried out at a surfactant concentration slightly above point M, the left-pointing cusp would be exited before entering the right one, i.e., the W minimum would disappear before the incipency of the O minimum. Hence the region between the cusp wedges corresponds to a single minimum potential, i.e., a one phase system, as in the ternary diagram.

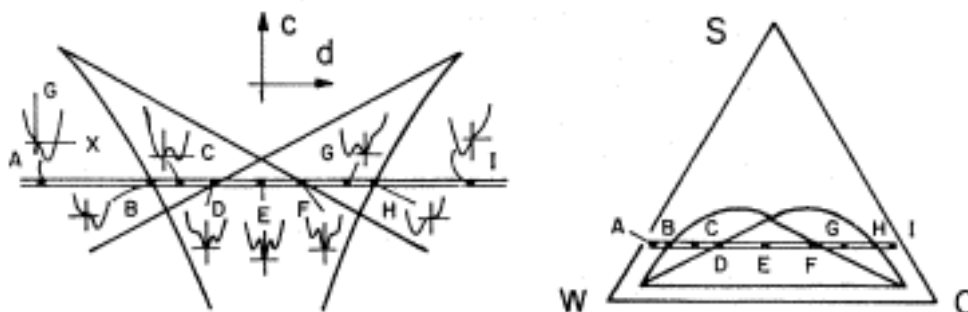


Figure 28. Phase behavior transitions due to a change of water/oil ratio interpreted on the butterfly catastrophe bifurcation and on a Winsor type III diagram. (From Ref. 110.)

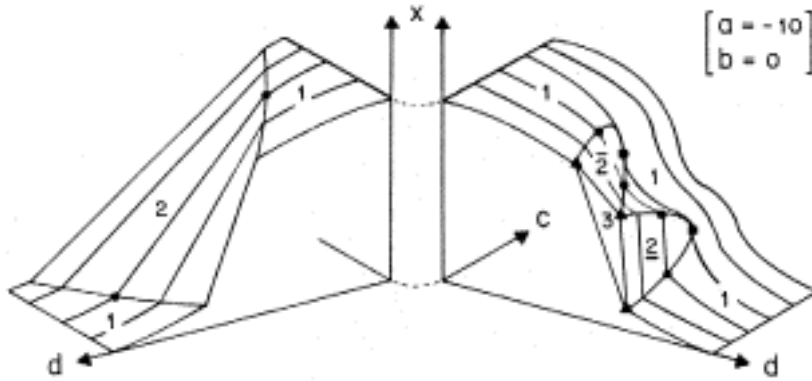


Figure 29. Butterfly catastrophe manifold $x(c,d)$ truncated after a Maxwell convention to render the phase behavior of Winsor type III diagram. (Adapted from Ref. 168.)

As with the cusp model and according to the Maxwell convention, the manifold (c,d) region corresponding to two or three minima of $G(x)$ is truncated away (see Fig. 29). In their nonoverlapping zone each of the cusps is replaced by a tie-line surface, the upper one of the $\bar{2}$ type, the lower one $\underline{2}$. In the zone of complete overlap the cusps are replaced by a tie triangle [168]. For c lower than the tie line between excess phases in the three-phase system (left portion), a 2-type tie-line surface identical to the case of Fig. 21 is drawn. For a better visualization, constant c lines are drawn on the truncated manifold. Figure 29 contains the same information as a Winsor Type III ternary diagram, with some additional data on the density of the phases in equilibrium.

3. Effect of Formulation

It was seen in Sec. I that a change in formulation may produce the transition I \rightarrow III \rightarrow II, or vice versa (see Fig. 3). It was also pointed out that such formulation effects may be represented by means of a single formulation variable SAD. Previous remarks in this section as well as Fig. 25 indicate that b has a symmetry-breaking effect similar to the negative of SAD. Figure 30 shows several (c,d) cuts of the bifurcation at different values of b . These cuts correspond to slices of the Fig. 24 ($a < 0$) surface. For values of b departing largely from zero, the (c,d) bifurcation becomes an asymmetrical cusp as in the $a > 0$ case seen previously (See. IV.B.1). For positive b the apex of the cusp is on the positive d side, i.e., the plait point of the two-phase region is near O as in Winsor Type I diagram, and conversely. As seen in Fig. 30 and detailed elsewhere [166,168], the variation of b from zero produces the shrinking of one of the cusps and the extension of the other. This is equivalent to the experimental data of Fig. 3, where a variation of formulation away from optimum produces the diminishing of one of the diphasic lobes and the spreading of the other. Hence it may be said that the role of the control variable b matches the effect of the formulation, more exactly, the effect of the negative of SAD.

The catastrophe model is symmetrical with respect to $(b = 0, d = 0)$, i.e., a change of sign of both b and d produces only a change of sign of x . Translated into phase behavior terminology, this means that the change of sign of SAD results in the swapping of the roles of O and W, as experimentally corroborated.

4. Quality of SOW System

By comparing the two bifurcation (b,c,d) cuts of Fig. 24, it is obvious that the control variable a determines the existence of the butterfly shaped bifurcation. For $a = 0$ and for $b = 0$ the butterfly bifurcation collapses into its lower cusp, i.e., the apices of the two overlapping cusps merge into a tricritical point [73,166].

For increasingly negative values of a , the butterfly bifurcation increases in size, while for positive values of a , three separate minima of G are never obtained. Translated into optimum Type III diagram equivalents, this means that when a tends to zero from a negative value, the two-phase $\bar{2}$ and $\underline{2}$ lobes and the three-phase region shrink, while the lower 2 region spreads over all of the multiphase zone. Such an effect has been observed with surfactant mixtures of hydrophilic and lipophilic components [22,109, 118]. The more different are the two components, the more they fractionate between phases [37,54,109,169]. At the limit, the hydrophilic component partitions in the W phase and the lipophilic component in the O phase, resulting in a two-phase SOW system of poor *quality* with roughly horizontal tie lines. Light alcohols, e.g., sec-butanol, produce roughly similar behavior, and they also may be considered as very poor surfactants [15,16].

Hence, control variable a may be viewed as some indication of the quality of the system (see Sec. I.F). Indeed, for increasingly negative values of a , the spinodal zone increasingly overlaps the binodal region, thus resulting in an overall free energy decrease [168]. However, the quality of a SOW system is still an unsettled matter, and the arguments above are essentially qualitative.

C. Interpretation of Emulsion Inversion

1. Selection of the Proper Model

It was seen in Sec. III that the cusp catastrophe model allows the interpretation of both the phase behavior and the emulsion inversion of a binary system with matching significance of the control variables.

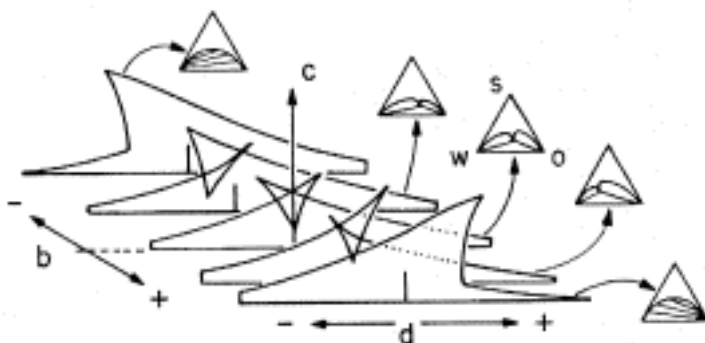


Figure 30. Sections at constant b of the butterfly catastrophe bifurcation for $a < 0$, and corresponding ternary diagrams.

Since the butterfly catastrophe renders the phase behavior of SOW ternaries, it is the proper model to investigate the emulsion inversion of these systems [166].

As in Sec. III.D, the perfect delay convention is the required selection, and state variable x may represent the curvature of the interface, taken as positive when the concavity is toward the oil phase (O/W emulsion). For the sake of simplicity x may also stand for an equivalent intrinsic property which is easier to grasp, i.e., the deviation of the density of the external phase of the emulsion from the average density of the O and W phases. Thus, positive x (respectively negative) would correspond to an O/W (respectively, W/O) two-phase emulsion. In three-phase systems the MOW symbol will be used. According to Brancroft's rules as stated in Sec. II-B, the external phase of an emulsion formed by stirring a pre-equilibrated system, i.e., an "initial emulsion," should be the phase with x value nearest zero, i.e., the surfactant-rich phase.

The discussion of the experimental data from Secs. II.C and II.D showed that the proper plot to study emulsion inversion is the formulation-water/oil ratio bidimensional map. From the Sec. IV.B interpretations, it is clear that this corresponds to the subspace of control variables b and d .

2. Representation of the Formulation-WOR Map

The effects of control variables b and d are to be investigated at constant a and c , i.e., quality and surfactant concentration. The nontrivial case differing from the simple cusp model corresponds to (a,c) values for which the system might exhibit up to three phases, i.e., negative a and a c value neither too high nor too low. Unless stated otherwise, the displayed graphic material corresponds to $a = -10$ and $c = 22.5$; in this case the representative point of the system is located near the center of the MLN triangle in Fig. 27, where both b and d are zero.

Figure 31 represents the manifold $x(b,d)$ cut of the butterfly catastrophe, which happens to be a surface composed of two overlapping cusps pointing at each other. The surface is symmetrical with respect to point $(x = 0, b = 0, d = 0)$. The negative b cusp is located mainly at $x \gg 0$, while the opposite applies to the positive b cusp.

The analysis of this manifold may be carried out in the same way as in previous cases, by observing the number of intersection points of a vertical line with the surface. Whether there are one, three, or five such points, the $G(x)$ potential exhibits one, two, or three minima, i.e., possible emulsion states. At sufficiently negative b and d , there is only one intersection on the positive x region of the surface, and conversely. The upper part of the surface ($x \gg 0$) thus corresponds to O/W emulsions, while the lower part represents W/O emulsions. In the central region where three states are available, the MOW label will be used. Depending on the characteristics of the occupied state, the MOW emulsion might be of the O/W or W/O type or neither.

The projection of the singularities on the control (b,d) subspace, i.e., the bifurcation (b,d) cut, is shown in Fig. 31, and reproduced in Fig. 32, together with a schematic formulation-WOR inversion map in matching axes. This bifurcation corresponds to a constant c horizontal cut of Fig. 24 across the self-intersecting region. Control variable b stands for the negative of generalized formulation SAD, while d represents the relative

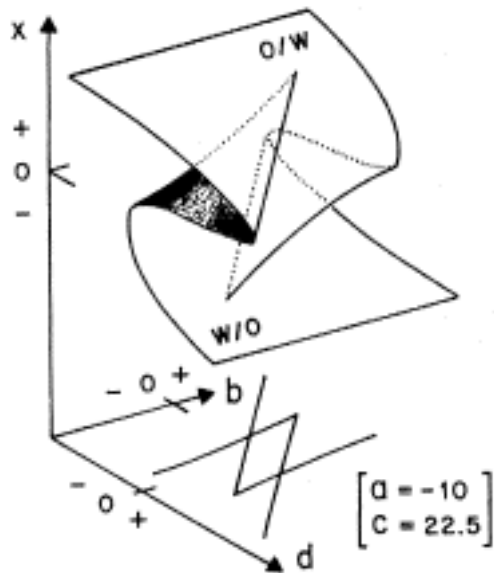


Figure 31. Butterfly catastrophe manifold $x(b,d)$ and bifurcation (b,d) cut.

amount of oil; as a consequence, the represented map fits Fig. 14 data but with the axis directions inverted. Again the topological similarity of the two maps is striking, and gives a hint that the hysteresis zones are probably related to the nonoverlapping region of the cusps (Fig. 32).

Because of the duality of the interpretation [166], it is worth remarking at once that these figures provide additional information on the phase behavior. At optimum formulation ($b = 0$), it is clear that a d scan from left to right would produce the changes displayed as path A-I in Fig. 28. Moreover, it is known experimentally that in the SAD/WOR map, the phase behavior at $SAD = 0$ changes from 3 to 1 at a very high content of any of the phases, because of the complete dissolution of one phase in the other [62,91]. This is just what the bifurcation model shows at $b = 0$, far from $d = 0$.

3. Catastrophic Inversion

When the water/oil ratio is changed at an off-optimum formulation, i.e., when SAD and b are far away from zero, the experimental evidence (see Fig. 14) indicates that the inversion location depends on the direction of the change. In Sec. II.D it was shown that this hysteresis phenomenon is interpreted quite accurately by catastrophe theory, specifically by the crossing of a cusp carried out with the perfect-delay convention.

It is clear from Figs. 31 and 32 that the (b,d) section of the butterfly catastrophe is composed of two cusps. The only difference from the Sec. II.D case is that these cusps are in a different subspace and show some slanting with respect to the coordinate axes. By changing d along a constant b line which does not cross the overlapping region of the two cusps, an inversion with hysteresis would occur in exactly the same way as in Fig. 22. Figure 33 indicates such an ABDE path for $b \ll 0$, i.e., positive SAD, together with

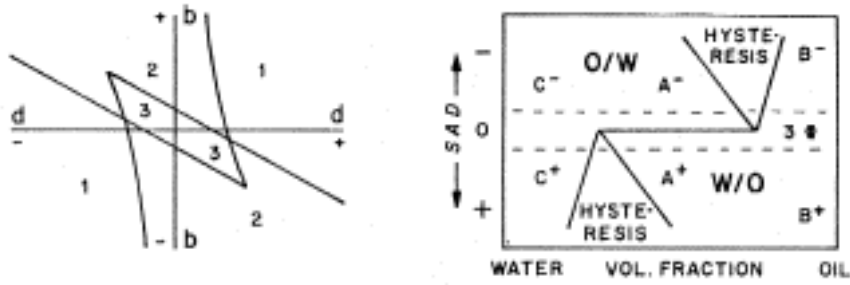


Figure 32. Butterfly catastrophe bifurcation (b,d) cut and formulation/WOR inversion map in matching axes.

the corresponding $G(x)$ graphs. The ball-in-the-hole analogy of Fig. 33 allows the interpretation of the inversion hysteresis. When the path is followed from A to E, the original emulsion type at A (O/W) is conserved until the corresponding state vanishes at D. A catastrophic inversion occurs at DD' with a jump in both G and x values of the current state. When the path is followed in the opposite direction from E to A, the inversion occurs at B'B. The BD part of the trajectory, i.e., the inside of the cusp, corresponds to a hysteresis zone. It is worth remarking that the width of the cusp increases when b shifts away from zero. The same qualitative trend is found in the Fig. 32 experimental data, in which this hysteresis zone is a wedge-shaped region vanishing at $SAD = 0$. Of course, the actual data do not necessarily correspond to a perfect-delay convention, but rather to a partial delay, as might be expected from systems submitted to random perturbations. Figure 34 shows the aspect of the manifold cuts, i.e., x versus d ,

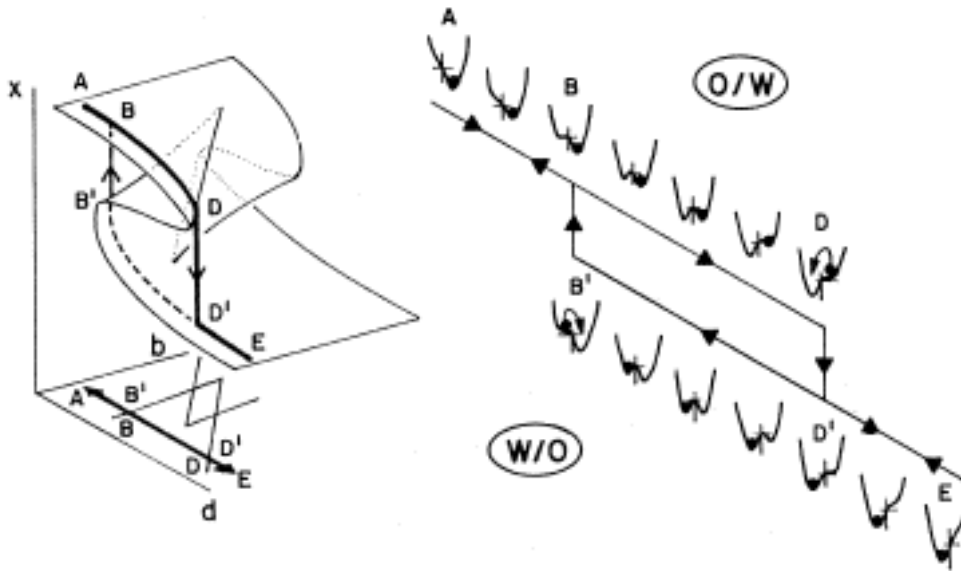


Figure 33. Catastrophic inversion due to a change in internal phase ratio, interpreted on the $x(b,d)$ manifold and by means of the ball-in-the-hole analogy.

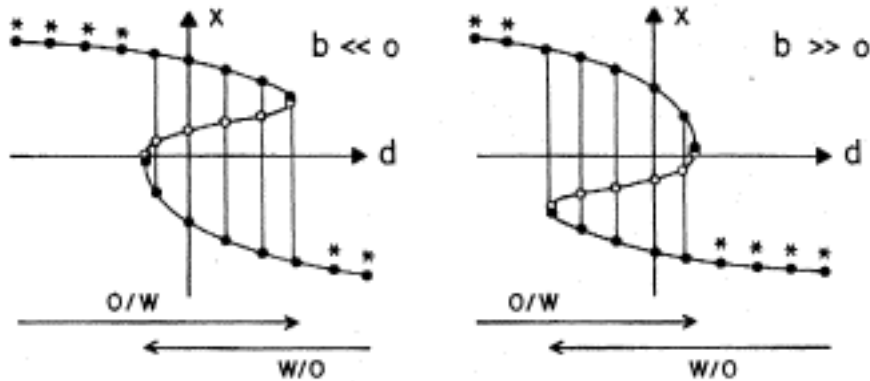


Figure 34. Cuts of the $x(b,d)$ manifold far away from b

far away from $b = 0$. The black dots indicate the minima of $G(x)$, i.e., the possible states. Out of the cusp fold there is only one possible state, noted by an asterisk. Inside the fold two states are possible; however, one of them may be more probable for physical reasons when the system is subjected to small perturbations as in actual cases, and when a non-perfect-delay convention might be the most reasonable approximation. This point needs further study, but a simple qualitative discussion may demonstrate the similarity of the model and the experimental data.

Let us take the $b \gg 0$ case and assume that a perturbation may be induced by an oscillation of the x value about the minimum. The wider the minimum, i.e., the farther it is from the adjoining maximum, the more stable or more probable the corresponding state. If this assumption is valid, it means that in the $b \gg 0$ case, the positive x minimum (O/W), which is more distant from the maximum (white dots) than the negative minimum (W/O), is more probable in the two-state zone. Translated into formulation /WOR map terms, it means that at negative SAD the O/W zone is more extended than the W/O. At $b \ll 0$ the opposite applies. As a consequence the actual hysteresis zone will be displaced to the right (positive d) at $b \gg 0$ and to the left (negative d) at $b \ll 0$, as found in the Fig. 32 experimental data. The fact that this displacement of the inversion branches has been found to increase when stirring is increased [140], i.e., when more perturbations are likely, seem s to support this suggestion.

The butterfly catastrophe model thus allows the interpretation of the inversion along the vertical branches of the locus. This inversion type may be definitely granted the designation "catastrophic" from its irreversibility and hysteresis features.

4. Transitional Inversion

When the formulation is changed in the center of the SAD/WOR map, the emulsion is experimentally found to invert from O/W to W/O, or vice versa, with no apparent discontinuity (see Sec. II.D). On the butterfly catastrophe manifold and bifurcation, this would correspond to a change of b at or near $d = 0$.

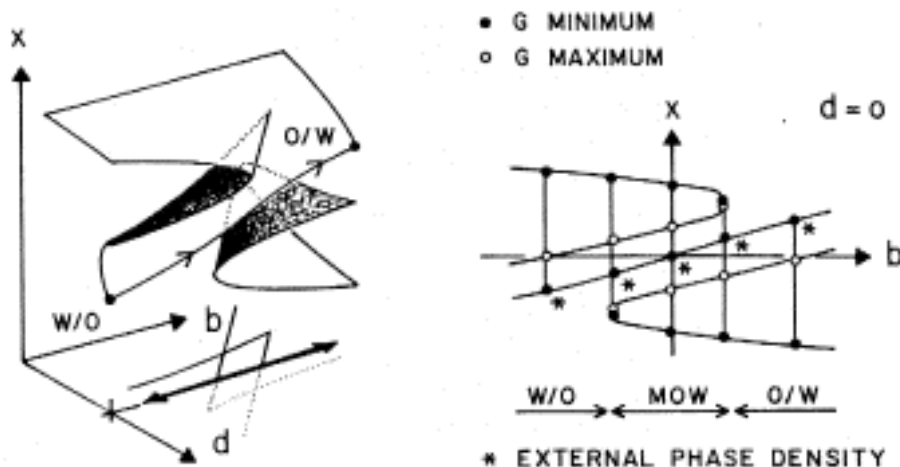


Figure 35. Butterfly catastrophe manifold $x(b,d)$ with the $d > 0$ portion removed, and $x(b,0)$ cut showing the path followed during a transitional inversion.

Figure 35 indicates the shape of the manifold section at $d = 0$, with the $d > 0$ portion removed. In the x versus b drawing, the black dots stand for $G(x)$ minima, i.e., possible states; the asterisks indicate the initial emulsion external phase according to the Bancroft rule, as stated in Sec. II.B, i.e., such that the external phase is the one with x value nearest zero. From this figure it is clear that the initial emulsion is W/O ($x < 0$) at $b < 0$ and conversely, i.e., it corresponds always to the surface central fold which rises from $x < 0$ at $b < 0$ to $x > 0$ at $b > 0$. Because of the application of the perfect-delay convention, the original state is maintained when a change occurs unless the corresponding minimum vanishes. The latter does not occur because of the continuity of the median fold. When b changes from negative to positive, i.e., SAD from positive to negative, the external phase remains the same but continuously changes its nature from O ($x < 0$) to W ($x > 0$). In three-phase MOW emulsions the model indicates a microemulsion external phase with two coexisting internal phases.

Figure 36 indicates the matching ball-in-the-hole analogy. When decreasing b along the ABCDE path, the original emulsion state at A ($b \gg 0$, $d = 0$) is O/W since the right minimum of $G(W)$ is closer to zero x than is the left one (O). When b is decreased, the current state position slowly shifts toward lower x values.

When the three-state region is attained at B, a new possible state appears at $x \gg 0$, i.e., an excess W phase. The current state becomes a MOW emulsion with a microemulsion external phase (M) and two excess phases (O and W).

At D the low x minimum vanishes, i.e., the oil excess phase disappears and in the remaining two-phase system the current state corresponds to the lower x minimum, i.e., to the O phase. The MOW emulsion has thus been transformed into a W/O type.

In the overall change, the microemulsion, which is the external phase, changes from W to O continuously; this occurs because the microemulsion solubilizes more and more of the O phase (and makes it disappear) and demixes a W excess phase. Such a change is continuous and reversible, and of course occurs in the same way in both directions with no hysteresis. These features strikingly match the experimental evidence about the so-

called transitional inversion, which is actually not an inversion but a continuous change of the microemulsion phase from O to W, or vice versa.

Such reasoning may be corroborated by considering the sequence of ternary diagrams as in the Fig. 3 scan. From these experimental data it is obvious that the surfactant-rich microemulsion phase continuously changes from O to W when the formulation is scanned.

5. Effect of Surfactant Concentration

The case dealt with previously corresponds to a value of c such that the representative point would lie in the center of the three-phase region at $b = 0$ and $d = 0$. In other words, the bifurcation (b,d) horizontal cut of the surface of Fig. 24 was realized below the self-intersection of the surface.

If the plane of cut rises, i.e., c increases, the overlapping of the cusps diminishes until the intercusp groove is reached. For higher values of c the two cusps become disjoined. Such a change is easily followed on the graphic of Fig. 27 by realizing a horizontal cut. For b different from zero (see Fig. 30) the same reasoning applies. Referring to the Fig. 27 nomenclature, three phases and MOW emulsions occur when the value of c corresponds to a cut between M and LN. Below that value a two-state system occurs, even when G has three minima, because the central minimum is higher than the lateral ones. Above point M, the constant c cut produces a one-phase system in the neighborhood of the optimum formulation. For c higher than the QR critical points a one-phase region is obtained at all values of d , for this particular value of b . It may be seen from Figs. 24 and 30 that this threshold value for monophasic systems increases when b departs from zero as the (c, d) bifurcation becomes asymmetrical. This matches the Bavière and Lipow criterion [114,115] for optimum formulation, i.e., minimum height of the multiphase zone of the ternary diagram.

Referring to Fig. 28, it is possible to "travel" from A (aqueous micellar solution) to I (oleic micellar solution) along a path passing outside the multiphase region, i.e., by a roundabout circuit inside the one-phase region. From Fig. 24, such a change may occur at constant c and d by changing the sign of b . Such paths are perfectly consistent with phase behavior studies. As far as the interpretation of the emulsion type is concerned, this would imply that single-state emulsions are in fact microemulsions, and that macroemulsions, correspond to two- and three-state cases.

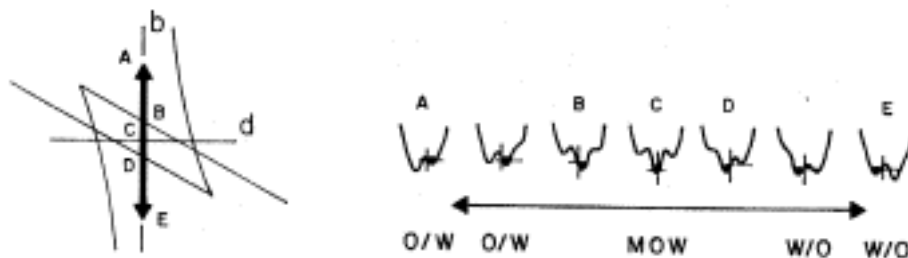


Figure 36. B all-in-the-hole analogy to interpret the transitional inversion.

The revisited Bancroft rule may be stated as follows: "The external phase of the initial macroemulsion obtained upon stirring an equilibrated multiphase SOW system is the micellar solution or the microemulsion phase." This ultimate detail allows a perfect fit between the two interpretations and the experimental results.

Acknowledgments

The author wishes to express his appreciation to Dr. P. Becher for encouraging him to carry out the early work on the catastrophe theory model, and to Ms. Nelia Pérez for her patience in typing the successive versions of the manuscript.

References

1. M. Schwartz, J. W. Perry, and J. Berch, *Surface Active Agents and Detergents*, Vol. II, Reprint, R. E. Krieger, Huntington, N.Y., 1977.
2. Davidsohn and B. Milwidsky, *Synthetic Detergents*, Halsted, New York, 1978.
3. M. J. Schick (ed.), *Nonionic Surfactants*, Marcel Dekker, New York, 1967.
4. W. H. Linfield (ed.), *Anionic Surfactants*, Marcel Dekker, New York, 1976.
5. E. Jungermann (ed.), *Cationic Surfactants*, Marcel Dekker, New York, 1969.
6. P. A. Winsor, *Solvent Properties of Amphiphilic Compounds*, Butterworth, London, 1954.
7. K. Shinoda (ed.), *Solvent Properties of Surfactant Solutions*, Marcel Dekker, New York, 1967.
8. W. Adamson, *Physical Chemistry of Surfaces*, 2nd ed., Wiley Interscience, New York, 1967.
9. J. J. Bikerman, *Physical Surfaces*, Academic, New York, 1970.
10. L. I. Osipow, *Surface Chemistry - Theory and Industrial Applications*, Reprint, R. E. Krieger, Huntington, N.Y., 1977.
11. P. Becher, *Emulsions - Theory and Practice*, 2nd ed., Reprint, R. E. Krieger, Huntington, N.Y., 1977.
12. M. J. Rosen, *Surfactants and Interfacial Phenomena*, Wiley, New York, 1978.
13. D. K. Chattorai and K. S. Birdi, *Adsorption and the Gibbs Surface Excess*, Plenum, New York, 1984.
14. K. Shinoda, *Principles of Solution and Solubility*, Marcel Dekker, New York, 1978.
15. M. Bavière, R. S. Schechter and W. H. Wade, in *Surface Phenomena in Enhanced Oil Recovery* (D. O. Shah, ed.), Plenum, New York, 1981.
16. M. Bavière, R. S. Schechter, and W. H. Wade, *J. Colloid Interface Sci.* 81: 266 (1981).
17. P. D. Fleming and J. E. Vinatieri, *J. Chem. Phys.* 66: 3147 (1977).
18. P. D. Fleming and J. E. Vinateri, Paper SPE 7582, *53rd Annual Fall Tech. Conf. Soc. Pet. Eng.*, Houston, Oct. 1978.
19. J. E. Vinateri and P. D. Fleming, *Soc. Pet. Eng. J.* 19: 289 (1979).
20. M. Bourrel and C. Chambu, *Soc. Pet. Eng. J.* 23: 327 (1983).

21. J. L. Salager, Ph.D. Dissertation, University of Texas, Austin, 1977.
22. C. Koukounis, M. S. Thesis, University of Texas, Austin, 1978.
23. M. Bourrel, C. Chambu, and F. Verzaro, *Proc. 2nd Eur. Symp. Enhanced Oil Recovery*, Technip, Paris, 1982, p. 39.
24. M. Bourrel, C. Chambu, R. S. Schechter, and W. H. Wade, *Soc. Pet. Eng. J.* 22: 28 (1982).
25. W. C. Griffin, *J. Soc. Cosmet. Chem.* 1: 311 (1949).
26. W. C. Griffin, *J. Soc. Cosmet. Chem.* 5: 249 (1954).
27. P. Becher, *J. Soc. Cosmet. Chem.* 11: 325 (1960).
28. P. Becher and R. L. Birkmeir, *J. Am. Oil Chem. Soc.* 41: 169 (1964).
29. P. Becher, in *Nonionic Surfactants* (M. J. Schick, ed.), MarcelDekker, New York, 1967, Chaps. 15 and 18.
30. P. Becher and W. C. Griffin, *HLB - A Bibliography 1940-1969*, Atlas Chemical Industries, 1970.
31. P. Becher and W. C. Griffin, in *McCutcheon's Detergents and Emulsifiers*, McCutcheon Division, MC Publishing Co., Glen Rock, N.J., 1974.
32. P. Becher, *J. Dispersion Sci. Technol.* 5: 81 (1984).
33. K. Shinoda and H. Saito, *J. Colloid Interface Sci.* 30: 258 (1969).
34. K. Shinoda, *Proc. 5th Int. Cong. Surf. Act.*, Barcelona, Spain, 2: 275 (1969).
35. Beerbower and J. Nixon, *Preprints Minneapolis Meet. Div. Pet. Chem. Am. Chem. Soc.*, Apr. 1969, p 62.
36. Parkinson and P. Sherman, *J. Colloid Interface Sci.* 41: 328 (1972).
37. Graciaa, J. Lachaise, J. G. Sayous, M. Bourrel, R. S. Schechter, and W. H. Wade, *Proc. 2nd Eur. Symp. Enhanced Oil Recovery*, Technip, Paris, 1982, p. 61.
38. Graciaa, Y. Barakat, M. EI-Emary, L. Fortney, R. S. Schechter, S. Yiv, and W. H. Wade, *J. Colloid Interface Sci.* 89: 209 (1982).
39. J., Lin, in *Colloid and Interface Science* (M. Kerker, ed.), 2: 431, Academic, New York, 1976.
40. J. Lin, *Tenside Deterg.* 17: 119 (1980).
41. R. C. Little, *J. Colloid Interface Sci.* 65: 587 (1978).
42. Lo., A. T. Florence, J. P. Treguier, M. Seiller, and F. Puisieux, *J. Colloid Interface Sci.* 59: 319 (1977).
43. K. Shinoda and H. Takeda, *J. Colloid Interface Sci.* 32: 642 (1970).
44. L. Marszall, *J. Colloid Interface Sci.* 60: 570 (1977).
45. L. Marszall, *J. Colloid Interface Sci.* 65: 589 (1978).
46. H. Kunieda, K. Hanno, S. Yamaguchi, and K. Shinoda, *J. Colloid Interface Sci.* 107: 129 (1985).
47. H. Kunieda and K. Shinoda, *J. Colloid Interface Sci.* 107: 107 (1985).
48. Beerbower and M. Hill, in *McCutcheon's Detergents and Emulsifiers*, McCutcheon Division, MC Publishing Co., Glen Rock, N.J., 1971, p. 223.
49. Beerbower and M. Hill, *Am. Cosmet. Perfum.* 87: 85 (1972).
50. J. H. Hildebrand and R. L. Scott, *Regular Solutions*, Prentice- Hall, Englewood Cliffs, N.J., 1962.
51. J. H. Hildebrand, J. M. Prausnitz, and R. L. Scott, *Regular and Related Solutions*, Van Nostrand Reinhold, New York, 1970.

52. F. Barton, *Handbook of Solubility Parameters and Other Cohesive Parameters*, CRC, Boca Raton, Fla., 1983.
53. H. Phelps, K. Bennett, H. T. Davis, and L. E. Scriven, Paper 116, *86th Annual Meet. AIChE*, Houston, Apr. 1979.
54. K. Chan and D. O. Shah, SPE Paper 7869, *Symp. Oil Field Geothermal Chem. Soc. Pet Eng.*, Houston, Jan. 1979.
55. R. L. Reed and R. N. Healy, in *Improved Oil Recovery by Surfactant and Polymer Flooding* (D. O. Shah and R. S. Schechter, eds.), Academic, New York, 1977, p. 383.
56. R. E. Antón, M. S. Thesis, Universidad de Oriente, Puerto La Cruz, Venezuela, 1981.
57. J. L. Salager, J. Morgan, R. S. Schechter, W. H. Wade, and E. Vasquez, *Soc. Pet. Eng. J.* 19: 107 (1979).
58. J. L. Salager, *Rev. Inst. Mex. Pet.* 11: 59 (1979).
59. E. Blevins, G. P. Willhite, and M. J. Michnick, Paper SPE 8260, *54th Annu. Fall Techn. Conf. Soc. Pet. Eng.*, Las Vegas, Nev., Sept. 1979.
60. J. Biaïis, B. Clin, and P. Lalanne, *C. R. Acad. Sci. Paris* 294-II: 497 (1982).
61. Huh, *Soc. Pet. Eng. J.* 23: 829 (1983).
62. H. Kunieda and K. Shinoda, *J. Colloid Interface Sci.* 75: 601 (1980).
63. R. N. Healy, R. L. Reed, and D. G. Stenmarck, *Soc. Pet. Eng. J.* 16: 147 (1976).
64. H. Saito and K. Shinoda, *J. Colloid Interface Sci.* 32: 647 (1970).
65. Vasquez, M. S. Thesis, University of Texas, Austin, 1978.
66. W. H. Wade, E. Vasquez, J. L. Salager, M. El-Emary, C. Koukounis and R. S. Schechter, in *Solution Chemistry of Surfactants* Vol. 2, (K. Mittal, ed.), Plenum, New York, 1979, p. 801.
67. R. L. Cash, J. L. Cayias, G. R. Fournier, J. K. Jacobson, C. A. LeGear, T. Schares, R. S. Schechter, and W. H. Wade, in *Detergents in the Changing Scene*, American Oil Chemists' Society, Champaign, Ill., 1977.
68. Anderson, M. Bidner, H. T. Davis, G. Manning, and L. E. Scriven, Paper SPE 5811, *Improved Oil Recovery Symp.*, Tulsa, Okla., Mar. 1976.
69. M. Bourrel, J. L. Salager, R. S. Schechter, and W. H. Wade, *J. Colloid Interface Sci.* 75:451 (1980).
70. M. Bellocq, J. Biaïis, B. Clin, A. Gelot, P. Lalanne, and B. Lemanceau, *J. Colloid Interface Sci.* 74: 311 (1980).
71. L. Wickert, G. P. Willhite, D. W. Green, and S. L. Black, Paper 45d, *85th Nat. Meet. AIChE*, Philadelphia, June 1978.
72. M. Bellocq, D. Bourbon, and B. Lemanceau, *J. Dispersion Sci. Technol.* 2: 27 (1981).
73. J. C. Lang and B. Widom, *Physica* 81A:190 (1975).
74. O. Shah and R. S. Schechter (eds.), *Improved Oil Recovery by Surfactant and Polymer Flooding*, Academic, New York, 1977.
75. R. T. Johansen and R. L. Berg (eds.), *Chemistry of Oil Recovery*, Am. Chem. Soc. Symposium Series No. 91, 1979.
76. O. Shah (ed.), *Surface Phenomena in Enhanced Oil Recovery*, Plenum, New York, 1981.

77. Wasan and A. Payatakes (eds.), *Interfacial Phenomena in Enhanced Oil Recovery*, AIChE Symposium Series No. 212, Vol. 78, 1982.
78. T. F. Moore and R. L. Slobod, *Producers Monthly* (Aug.) : 20 (1956).
79. J. J. Taber, *Soc. Pet. Eng. J.* 9: 3 (1969).
80. J. Lefebvre du Prey, *Soc. Pet. Eng. J.* 13: 39 (1973).
81. J. C. Melrose and C. F. Brandner, *Can. J. Pet Technol.* 13: 54 (1974).
82. J. C. Noronha and D. O. Shah, in *AIChE Symposium Series* No. 212,78: 42 (D. Wasan and A. Payatakes, eds.), 1982.
83. Thurston, J. L. Salager, and R. S. Schechter, *J. Colloid Interface Sci.* 70: 517 (1979).
84. W. J. Benton, T. Fort, and C. A. Miller, Paper SPE 7579, *53rd Annual Fall Techn. Conf. Soc. Pet. Eng.*, Houston, Oct. 1978.
85. M. Cazabat, D. Langevin, J. Meunier, and A. Pouchelon, *Adv. Colloid Interface Sci.* 16:175 (1982).
86. O. Shah, K. S. Chan, and V. K. Banzal, *83rd Nat. Meet. AIChE*, Mar. 1977.
87. M. Y. Chiang, K. S. Chan, and D. O. Shah, *J. Can. Pet. Technol.* 17: 1 (1978).
88. J. Derderian, J. E. Glass, and G. M. Bryant, *J. Colloid Interface Sci.* 68: 184 (1979).
89. Pouchelon, D. Chatenay, J. Meunier, and D. Langevin, *J. Colloid Interface Sci.* 82: 418 (1981).
90. R. L. Reed and R. N. Healy, Paper SPE 8262, *54th Annual Fall Techn. Conf. Soc. Pet. Eng.*, Las Vegas, Nev., Sept. 1979.
91. K. Shinoda and M. Saito, *J. Colloid Interface Sci.* 26:70 (1969).
92. W. H. Wade, J. C. Morgan, J. K. Jacobson and R. S. Schechter, *Soc. Pet. Eng. J.* 17:122 (1977).
93. M. C. Puerto and W. W. Gale, *Soc. Pet. Eng. J.* 17: 193 (1977).
94. L. Cash, J. L. Cayias, G. Fournier, D. McAllister, T. Schares, R. S. Schechter, and W. H. Wade, *J. Colloid Interface Sci.* 59: 39 (1977).
95. W. C. Hsieh and D. O. Shah, Paper SPE 6594, *Symp. Oil Field Geothermal Chem. Soc. Pet. Eng.*, La Jolla, Calif., June 1977.
96. S. J. Salter, Paper SPE 6843, *52nd Annual Fall Techn. Conf. Soc. Pet. Eng.*, Denver, Colo., Oct. 1977.
97. K. Shinoda and H. Kunieda, in *Microemulsions -Theory and Practice* (L. M. Prince, ed.), Academic, New York, 1977.
98. W. H. Wade, J. C. Morgan, R. S. Schechter, J. K. Jacobson, and J. L. Salager, *Soc. Pet. Eng. J.* 18: 242 (1978).
99. M. E. Hayes, Ph.D. Dissertation, University of Texas, Austin, 1978.
100. M. E. Hayes, M. El-Emary, R. S. Schechter, and W. H. Wade, *J. Colloid Interface Sci.* 68: 591 (1979).
101. M. E. Hayes, M. Bourrel, M. El-Emary, R. S. Schechter, and W. H. Wade, *Soc. Pet. Eng. J.* 19: 349 (1979).
102. J. L. Salager, M. Bourrel, R. S. Schechter, and W. H. Wade, *Soc. Pet. Eng. J.* 19: 271 (1979).
103. W. Malmberg, C. C. Gajderowicz, F. D. Martin, J. S. Ward, and J. J. Taber, Paper SPE 8323, *54th Annual Fall Techn. Conf. Soc. Pet. Eng.*, Las Vegas, Nev., Sept. 1979.
104. M. C. Puerto and R. L. Reed, *Soc. Pet. Eng. J.* 23: 669 (1983).

105. J. L. Cayias, R. S. Schechter, and W. H. Wade, *Soc. Pet. Eng. J.* 16: 351 (1976).
106. R. Glinsmann Paper SPE 8326, *54th Annual Fall Techn. Conf. Soc. Pet. Eng.*, Las Vegas, Nev., Sept. 1979.
107. M. K. Tham, and P. B. Lorenz, *Eur. Symp. Enhanced Oil Recovery*, Bournemouth, England, Sept. 1981.
108. M. Bourrel, J. L. Salager, R. S. Schechter, and W. H. Wade, *Colloq. Nat. CNRS* 938: 338 (1979).
109. M. Bourrel, C. Koukounis, R. S. Schechter, and W. H. Wade, *J. Dispersion Sci. Technol.* 1:13 (1980).
110. J. L. Salager, *Proc. First Int. Symp. Enhanced Oil Recovery*, INPELUZ, Maracaibo, Venezuela, Feb. 1985.
111. M. Bourrel, J. L. Salager, A. Lipow, R. S. Schechter, and W. H. Wade, Paper SPE 7450, *53rd Annual Fall Techn. Conf. Soc. Pet. Eng.*, Houston, Oct. 1978.
112. N. Moreno, M. S. Thesis, Universidad de Los Andes, Mérida, Venezuela (1986).
113. Huh, *J. Colloid Interface Sci.* 71: 408 (1979).
114. M. Bavière, Paper, SPE 6000, *51st Annual Fall Techn. Conf. Soc. Pet. Eng.*, New Orleans, La., Oct. 1976.
115. Lipow, M. Bourrel, R. S. Schechter, and W. H. Wade, *86th Nat. Meet. AIChE*, Houston, Apr. 1979.
116. Y. Barakat, L. Fortney, C. Lalanne-Cassou, R. S. Schechter, and W. H. Wade, Paper SPE/DOE 10679, *3rd Joint Symp. Enhanced Oil Recovery*, Dallas, Apr. 1982.
117. Graciaa, L. Fortney, R. S. Schechter, W. H. Wade, and S. Yiv, *Soc. Pet. Eng. J.* 22:743 (1982).
118. Martinez, M. S. Thesis, Universidad de Los Andes, Mérida, Venezuela (1986).
119. L. E. Scriven, in *Micellization, Solubilization and Microemulsions* (K. Mittal, ed.), Plenum, 1977, p. 877.
120. P. G. de Gennes and C. Taupin, *J. Phys. Chem.* 86: 2294 (1982).
121. Pouchelon, J. Meunier, D. Langevin, D. Chatenay, and A. M. Cazabat, *Chem. Phys. Lett.* 76: 277 (1980).
122. R. E. Antón and J. L. Salager, *J. Colloid Interface Sci.* 111: 54 (1986).
123. R. E. Antón, J. M. Andérez, and J. L. Salager, *Proc. First Int. Symp. Enhanced Oil Recovery*, INPELUZ, Maracaibo, Venezuela, Feb. 1985.
124. P. Sherman, *Emulsion Science*, Academic, New York, 1968.
125. T. J. Lin, *J. Soc. Cosmet. Chem.* 19: 683 (1968).
126. T. J. Lin and J. C. Lambrechts, *J. Soc. Cosmet. Chem.* 20: 185 (1969).
127. T. J. Lin, *J. Soc. Cosmet. Chem.* 21: 365 (1970).
128. P. Becher, *J. Soc. Cosmet. Chem.* 9: 141 (1958).
129. S. Friberg, *Food Emulsions*, Marcel Dekker, New York, 1982.
130. M. Bourrel, A. Graciaa, R. S. Schechter, and W. H. Wade, *J. Colloid Interface Sci.* 72: 161 (1979).
131. L. Salager, L. Quintero, E. Ramos, and J. M. Andérez, *J. Colloid Interface Sci.* 77: 288 (1980).
132. L. Salager, I. Loaiza- Maldonado, M. Miñana-Pdrez, and F. Silva, *J. Dispersion Sci. Technol.*, 3: 279 (1982).
133. W. D. Bancroft, *J. Phys. Chem.* 17: 501 (1913).

134. L. Salager, M. Miñana-Pérez, M. Pérez-Sánchez, M. Ramírez-Gouveia, and C. I. Rojas, *J. Dispersion Sci. Technol.* 4: 313 (1983).
135. Shinoda and H. Arai, *J. Colloid Interface Sci.* 25: 429 (1967).
136. Kunieda and K. Shinoda, *J. Colloid Interface Sci.* 70: 577 (1979).
137. R. E. Antón, P. Castillo, and J. L. Salager, *J. Dispersion Sci. Technol.* 7: 319 (1986)
138. P. Castillo, Thesis, Universidad de Los Andes, Mérida, Venezuela (1984).
139. L. Salager, M. Miñana-Pérez, J. M. Andérez, J. L. Grosso, C. I. Rojas, and I. Layrisse, *J. Dispersion Sci. Technol.* 4: 161 (1983).
140. P. Jarry, M. Miñana-Pérez, J. L. Salager, in *Surfactants in Solution*, Vol. 6, (K. Mittal, ed.), Plenum, New York, 1987, p. 1689.
141. Miñana-Pérez, P. Jarry, M. Pérez-Sánchez, M. Ramírez-Gouveia, and J. L. Salager, *J. Dispersion Sci. Technol.* 7: 331 (1986)
142. Boyd, C. Parkinson, and P. Sherman, *J. Colloid Interface Sci.* 41: 359 (1972)
143. S. Vijayan, C. Ramachandran, H. Doshi, and D. O. Shah, in *Surface Phenomena in Enhanced Oil Recovery* (D. O. Shah, ed.), Plenum, New York, 1981.
144. E. Vinateri, *Soc. Pet. Eng. J.* 20: 402 (1980).
145. S. Milos and D. T. Wasan, *Colloids Surf.* 4: 91 (1982).
146. M. Baldauf, R. S. Schechter, W. H. Wade, and A. Graciaa, *J. Colloid Interface Sci.* 85: 187 (1982).
147. J. L. Salager, J. L. Grosso, and M. A. Eslava, *Rev. Tecn. INTEVEP* 2:149 (1982).
148. T. Wasan, S. M. Shah, N. Aderangui, M. Chan, and J. J. McNamara, Paper SPE 6846, *52nd Annual Fall Techn. Conf. Soc. Pet. Eng.*, Denver, Colo., Oct. 1977.
149. Moreno, Thesis, Universidad de Los Andes, Mérida, Venezuela (1983).
150. Nava, MSc Thesis, Universidad de Los Andes, Mérida, Venezuela (1984).
151. Silva, MSc Thesis, Universidad de Los Andes, Mérida, Venezuela (1984).
152. Ramírez-Gouveia, M.S. Thesis, Universidad de Los Andes, Mérida, Venezuela (1985)
153. S. Nagata, *Mixing Principles and Applications*, Kodansha (Halsted Press), Tokyo, 1975.
154. Dickinson, *J. Colloid Interface Sci.* 87: 416 (1982).
155. J. W. Cahn, *Acta Metall.* 9: 795 (1961).
156. J. W. Cahn, *Acta Metall.* 10: 179 (1962).
157. J. W. Cahn, *J. Chem. Phys.* 42: 93 (1965).
158. J. W. Cahn, *Acta Metall.* 14: 1685 (1966).
159. J. W. Cahn, *Trans. AIME* 242: 166 (1968).
160. R. Thom, *Stabilité Structurelle et Morphogénèse*, Benjamin, New York, 1972 (expanded English translation, 1975).
161. E. C. Zeeman, *Sci. Am.* 234: 65 (1976).
162. L. Benguigui and L. S. Schulman, *Phys. Lett. A* 45: 315 (1973).
163. T. Poston and I. Stewart, *Catastrophe Theory and Its Applications*, Pitman, London, 1978.
164. J. M. Prausnitz, *Molecular Thermodynamics of Fluid Phase Equilibria*, Prentice-Hall, Englewood Cliffs, N.J., 1969.

165. E. Dickinson, *J. Colloid Interface Sci.* 84:284 (1981).
166. J. L. Salager, in *Surfactants in Solution*, Vol. 4, (K. Mittal, ed.), Plenum, New York. 1986, p. 439.
167. T Davis and L. E. Scriven, Paper SPE 9278, *55th Annual Fall Techn. Conf. Soc. Pet. Eng.*, Dallas, Sept. 1980.
168. J. L. Salager, *J. Colloid Interface Sci.* 105: 21 (1985).
169. Koukounis, W. H. Wade, and R. S. Schechter, *Soc. Pet. Eng. J.* 23: 301 (1983).